Article:
Bellasio, C. and Griffiths, H. (2013) The operation of two decarboxylases, transamination, and partitioning of C4 metabolic processes between mesophyll and bundle sheath cells allows light capture to be balanced for the maize C4 pathway. Plant Physiology, 164 (1). 466 - 480. ISSN 0032-0889

https://doi.org/10.1104/pp.113.228221

Plant Physiology

The operation of two decarboxylases (NADPME and PEPCK), transamination and partitioning of C_4 metabolic processes between mesophylll and bundle sheath cells allows light capture to be balanced for the maize C_4 pathway

Chandra Bellasio and Howard Griffiths

Physiological Ecology Group, Department of Plant Sciences, University of Cambridge, Downing Street, Cambridge, CB2 3EA, UK.

Correspondence: chandra.bellasio@plantsci.cam.ac.uk

Abstract:

The C_4 photosynthesis carbon concentrating mechanism (CCM) in maize has two CO_2 delivery pathways to the Bundle Sheath (BS) (respectively via malate, MAL or aspartate, ASP), and rates of PGA reduction, starch synthesis and PEP regeneration also vary between BS and Mesophyll (M) cells. The theoretical partitioning of ATP supply between M and BS cells was derived for these metabolic activities from simulated profiles of light penetration across a leaf, with a potential 3-fold difference in the fraction of ATP produced in the BS relative to M, (from 0.29 to 0.96). A steady-state metabolic model was tested using varying light quality to differentially stimulate M or BS photosystems. CO_2 uptake, ATP production rate (J_{ATP} derived with a low O_2 / chlorophyll fluorescence method) and carbon isotope discrimination were measured on plants under a low light intensity, which is considered to affect C_4 operating efficiency. The light quality treatments did not change the empirical ATP cost of gross assimilation (J_{ATP} / GA). Using the metabolic model, measured J_{ATP} / GA was compared to the predicted ATP demand as metabolic functions were varied between M and BS. Transamination and the two decarboxylase systems (NADPME and PEPCK) were critical for matching ATP and NADPH demand in BS and M when light capture was varied under contrasting light qualities.

Keywords

Bundle sheath, C_4, isotopic discrimination, leakiness, mesophyll, light penetration profiles, Δ13C.

Introduction

Interest in the C_4 pathway has been increased by the potential for enhancing crop productivity and maintaining yield stability in the face of global warming and population pressure (Friso et al., 2010; Zhu et al., 2010; Covshoff and Hibberd, 2012). Maize (Zea mays, L.), a C_4 plant of the NADP-ME subtype, is a leading grain production cereal (FAO, 2012). C_4 photosynthesis is a shared activity between mesophyll (M, abbreviations listed in Table 1) and bundle sheath (BS) cells, coupled to allow the operation of a biochemical carbon concentrating mechanism (CCM). The CCM effectively minimizes photorespiration by increasing the CO_2 concentration in BS (C_{BS}), where Rubisco is exclusively expressed. Since BS and M are connected by plasmodesmata, some CO_2 retrodiffuses. The refixation of that escaping CO_2 by the CCM increases the activity of the CCM and the total ATP demand ($ATP_{BS} + ATP_M$) for gross CO_2 assimilation (GA), ($ATP_{BS} + ATP_M$) / GA), from a theoretical minimum of 5 ATP (Furbank et al., 1990). Leakiness (Φ), the amount of CO_2 retrodiffusing relative to PEP carboxylation rate, is therefore a proxy for the coordination between the CCM and assimilatory activity (Henderson et al., 1992; Tazoe et al., 2006; Tazoe et al., 2008; Kromdijk et al., 2010; Ubierna et al., 2011; Bellasio and Griffiths, 2013).

Recently, the maize C_4 subgroup has been shown to be complicated by the presence of two BS decarboxylation enzyme systems (NADP-ME and PEP carboxykinase, PEPCK), presumably both acting as CO_2 delivery pathways (respectively via malate, MAL or aspartate, ASP) (Furumoto et al., 1999; Wingler et al., 1999; Furumoto et al., 2000; Eprintsev et al., 2011; Furbank, 2011; Pick et al., 2011). There is also an extensive overlap between BS and M functions since both cell types can synthesize starch (Spilatro and Preiss, 1987; Kanai and Edwards, 1999) and reduce phosphoglyceric acid, PGA (Majeran and van Wijk, 2009) (see the overall scheme in Fig. 1). Additionally, energetic partitioning can also vary between cell types, since the total ATP produced (J_{ATP}) per CO_2 fixed in GA (J_{ATP} / GA) may be produced in BS (mainly through cyclic electron flow around PSI) or in M (mainly through linear electron flow) depending on the light locally available in BS or M (Kramer and Evans, 2011; Yin and Struik, 2012). Furthermore, although all NADPH is produced in M, the only compartment operating linear electron transport and oxidising water, some NADPH is exported to BS through MAL diffusion, to meet the reducing power demand therein ($NADPH_{BS}$). To capture the complex C_4 physiology, several models of C_4 photosynthesis have been developed (Berry and Farquhar, 1978; Laisk and Edwards, 2000; von Caemmerer, 2000; Laisk and Edwards, 2009). The earlier approaches were developed into the von Caemmerer (2000) C_4 model. In particular the associated light limited equations (referred subsequently as the 'C_4 model'), are used to estimate the parameters needed to resolve the isotopic discrimination model, widely employed to study leakiness under low light conditions [for review see (Ubierna et al., 2011)]. The C_4 model partitions J_{ATP} into two fractions: i) the ATP consumed by PEP carboxylase (PEPC) and ii) the ATP consumed by the C_3 activity (glyoxylate recycling, PGA reduction, and RuBP regeneration). These activities are located in M, BS or in both compartments (see the overall

scheme in Figure 1). However, the C_4 model simplifies the spatial compartmentalization between BS and M, and in this paper we now develop the energetic implications of the differential contribution of M and BS to C_4 photosynthesis under different light regimes.

Because of these anatomical, metabolic and energetic complexities, C_4 metabolism is highly sensitive to limiting light intensity (Bellasio and Griffiths, 2013), and potentially light quality (Evans et al., 2007). Light quality has a greater influence on C_4 photosynthesis than on C_3. Leaf pigments preferentially absorb the blue and red region of the spectra and some wavelengths penetrate deeper into leaves. It was shown in C_3 leaves that exposure to different wavelengths results in characteristic light penetrations profiles, which translated into different gradients in photosystem II yield, rates of ATP production and assimilation (A) within the leaf (Terashima et al., 2009). In C_4 leaves, because of the concentric anatomy, light reaches M cells before the deeper BS (Evans et al., 2007), and could alter the balance between light harvesting and energetic partitioning between BS and M.

In this paper, we model the likely profiles of light penetration for specific wavelengths associated with Red, Green and Blue (R, G, B) light within a maize M and BS leaf cross section, and calculate the impact on potential ATP production for each cell type. We calculate the proportion of absorbed light (AB) for each wavelength, expressed as AB BS / M, the fraction of photons absorbed in BS relative to the photons absorbed in M, from which we derive J_{ATPBS} / J_{ATPM}, the fraction of ATP produced in BS relative to the ATP produced in M. Secondly, we developed a steady-state metabolic model (Fig. 1, Table 2), which augments the conventional C_4 model (von Caemmerer 2000), to capture the spatial separation between BS and M and partitions the ATP demand between BS and M cells in terms of PGA reduction (PR), starch synthesis (SS) and PEP regeneration, so as to meet the ATP availability in each cell type (Evans et al., 2007). Thirdly, photosynthetic characteristics (leaf level ATP production rate, CO_2 assimilation, stomatal conductance and Φ derived from on-line carbon isotope discrimination) were measured under R, G, B, and RGB in combination, using a decreasing photon flux density (from 500 to 50 $\mu E\ m^{-2}\ s^{-1}$) to investigate the importance of metabolic plasticity under limiting light intensities.

For instance, AB BS / M and J_{ATPBS} / J_{ATPM}, were both lower under the blue wavelengths (460 nm), which are rapidly extinguished within the M leaf profile, than under white light, confirming that light quality perturbs C_4 energetics. In spite of this shift, when maize plants were exposed to different light qualities there was no change in Φ indicating that, at steady state, the co-ordination between CCM activity and Rubisco assimilation was retained (Sun et al., 2011; Ubierna et al., 2011). The modelled metabolic plasticity projected a window for ATP demand partitioning, ATP_{BS} / ATP_M, which matched the values for J_{ATPBS} / J_{ATPM} supply estimated under B, G and R wavelengths. We show that the plasticity of C_4 metabolism, and in particular the possibility of shifting between malate and aspartate as primary carboxylase product, were of pivotal importance in allowing plasticity of ATP and NADPH demand. In conclusion, our study explains the extensive overlap between BS and M functions and the requirement for at least two

decarboxylase systems in NADP-ME subtype plants such as maize, providing an explanation for empirical observations on diversity of decarboxylase activities and PEP regeneration pathways (Rathnam, 1978; Chapman and Hatch, 1981; Wingler et al., 1999; Eprintsev et al., 2011; Furbank, 2011; Pick et al., 2011).

Results

Metabolic modelling of partitioning between BS and M.

The complexity of C_4 biochemistry (Furbank, 2011) was first integrated in a comprehensive steady-state model (Fig. 1), with key processes described by rate equations (Fig. 1, Box; Table 2) and associated ATP demand (Eqn. 11-13 in Table 2). This model captures the spatial separation between BS and M, the different pathways of the CCM (through ASP and MAL), the different carboxylating enzymes and the process of starch synthesis, as a means to develop the traditional C_4 model (von Caemmerer 2000). The metabolic model (Fig. 1) was generated on the assumption that ATP does not freely diffuse between BS and M and any light-induced J_{ATPBS} / J_{ATPM} fluctuations have to be countered by changing the partitioning of ATP demand (for a list of abbreviations see Table 1). Fig. 1 depicts the reactions which are localized in BS, in M or in both compartments. RuP phosphorylation is uniquely localized in BS to supply RuBP directly in proximity to Rubisco, and facilitate the substrate saturation of the Enzyme. Glyoxylate recycling is also a BS exclusive reaction (Fig. 1) (Yoshimura et al., 2004). This feature contributes to the CCM (the so called C_2 cycle) and, in an evolutionary perspective, it was acquired at an early stage (Sage et al., 2012; Schulze et al., 2013). PEP regeneration through PEP carboxykinase (PEPCK) is located uniquely in BS (Wingler et al., 1999), while PEP regeneration through pyruvate phosphate dikinase (PPDK), is located primarily in M (Fig. 1) (Friso et al., 2010; Majeran et al., 2010), and any PPDK activity in BS is generally neglected (von Caemmerer, 2000) (see also discussion). PGA reduction (PR), respiration, and starch synthesis (SS) are processes located both in BS and M (Spilatro and Preiss, 1987; Kanai and Edwards, 1999; Majeran and van Wijk, 2009; Friso et al., 2010).

These processes are described in detail below, after an initial comparison of modelled light profiles and measured photosynthetic characteristics under R, G and B wavelengths, to give a quantitative description of the biochemical mechanisms underpinning acclimation, fluxes and reaction rates, the dynamics of Φ and the effects on the total and relative ATP demand for assimilation.

Effect of light quality on ATP production in BS and M.

To study the influence of light quality on ATP production partitioning, J_{ATPBS} / J_{ATPM}, we first modelled C_4 anatomy (Fig. 2 left). Light penetration was modelled in two characteristic profiles

using the absorption-scattering theory (Fig. 2 right). Profiles were calibrated with leaf transmittance and reflectance at different wavelengths. Blue light was strongly absorbed (steep profile), green light was weakly absorbed (gradual profile) while red light had an intermediate profile of light penetration. These three profiles were integrated to estimate the contribution of absorbtance within abaxial + abaxial mesophyll, interveinal mesophyll and bundle sheath (Fig.2), and calculated the partitioning of absorbed light (AB) in BS and M (AB BS / M) under five relevant conditions (Table 3). AB BS / M was used in turn to estimate the partitioning of ATP production, J_{ATPBS} / J_{ATPM} (Table 3) under the assumption that photochemical yield did not vary through the leaf profile (see 'Estimated ATP production partitioning' in Material and Methods). At 400 nm, AB BS / M was lowest, representing J_{ATPBS} / J_{ATPM} of 0.29; at 540 nm, AB BS / M was highest together with J_{ATPBS} / J_{ATPM} (0.96). Under blue light, J_{ATPBS} / J_{ATPM} was close to the lowest value (0.31), increasing under red (0.68), natural white light (0.76) and green light (0.80). These values were derived independently of light intensity so they can be considered to reflect the actual ATP availability in BS and M under a wide range of light intensities. Since ATP does not diffuse between BS and M, and has a relatively small pool, at steady state, J_{ATPBS} / J_{ATPM} can be directly compared to the ATP demand partitioning, ATP_{BS} / ATP_{M}. For this comparison, the values for J_{ATPBS} / J_{ATPM} under blue, red, white and green light were used subsequently to plot Fig. 4 B. The model predicts that light quality will unbalance the partitioning of ATP production, and a comprehensive ecophysiological investigation was therefore used to compare gross assimilation and ATP supply and partitioning between B and M cells.

Effect of light quality on assimilatory traits.

Figure 3 shows the responses of maize to different light qualities (Red, R; Green, G; Blue, B; or RGB combined) measured under decreasing irradiance. Net assimilation (A), measured through gas exchange (Fig. 3 A), and J_{ATP} (Fig. 3 B) measured with the low O_2 - ETR method using a saturating light pulse, were significantly higher under R light and decreased under RGB, G and B. Light quality had no significant effect on stomatal conductance (g_s, Supplementary Fig. S 1 A), but Ci / Ca was lower under R light (Supplementary Fig. S 1 B) as a consequence of the higher A. The CO_2 concentration in BS (C_{BS}), estimated by fitting a C_4 photosynthesis model to J_{ATP}, was higher under R and G light (Supplementary Fig. S 1 C), because of the higher A. The light compensation point (LCP), bundle sheath conductance (g_{BS}) and respiration in the light (R_{LIGHT}) were not significantly influenced by light quality (Table 4).

With the precise estimate of R_{LIGHT} and J_{ATP}, we calculated J_{ATP} / GA, which represents the experimentally-determined ATP cost for gross assimilation. J_{ATP} / GA was not influenced by light intensity but varied between light qualities from 5.37 to 5.73, under B, R, RGB and G light. J_{ATP} / GA was then used in Fig. 4 B, plotted against the ATP production partitioning J_{ATPBS} / J_{ATPM}, found above. The relatively minor increase in J_{ATP} / GA (c 0.3 ATP / CO_2) observed

experimentally contrasts with the metabolic disruption theoretically predicted under these conditions (Evans et al., 2007). Our data was supported by real-time isotopic discrimination, Δ (Fig. 3 C) and leakiness, Φ (Fig. 3 D), which were not influenced by light quality, showing that the plant coped with a 2.5x shift in J_{ATPBS} / J_{ATPM} without any imbalance in the co-ordination of CCM activity and assimilation. Obtaining Φ data under such low light intensities represents a technical challenge and the experimental protocol was carefully optimised for low light intensity (Bellasio and Griffiths, 2013). Data obtained under low light are subject to a potential error magnification proportional to ξ [supporting figure S3, (Evans et al., 1986)], as clearly shown by the large error bars in Fig. 3D, and therefore should be interpreted with care. Leakiness, J_{ATP} / GA and the window of J_{ATPBS} / J_{ATPM} formed the basis of a metabolic model used to describe these biochemical responses.

Influence of BS activity on assimilatory metabolism and ATP demand (total and relative).

The comprehensive metabolic model (Fig. 1) was developed to describe the biochemical reactions directly and indirectly involved in C_4 assimilation by rate equations (Table 2). The proportions of three assimilatory ATP-consuming processes [starch synthesis (SS), phosphoglyceric acid reduction (PR) and PEP carboxykinase (PEPCK)] were manipulated to increase within BS (allocated, Fig. 4 A). These processes overlap between BS and M and could be allocated to BS without influencing the overall assimilation rate. By means of this progressive allocation, we predicted: i) the minimum and maximum ATP demand partitioning, ATP_{BS} / ATP_M (Eqn. 12 / Eqn. 13, Table 2); ii) the reaction rates and metabolite fluxes at a given ATP_{BS} / ATP_M, including the rate PEPCK and PPDK, the relative CO_2 flux through ASP and MAL and the partitioning of PGA reduction between BS and M; iii) the dynamics of total ATP demand for gross assimilation (ATP_{BS} + ATP_M) / GA at variable ATP_{BS} / ATP_M.

When the BS allocation rate of PR, PEPCK and SS was zero (referred as condition 1, number 1 in Fig. 1 and Fig. 4 B), the predicted ATP_{BS} / ATP_M was lowest (0.27). This value was comparable to J_{ATPBS} / J_{ATPM} resolved from the optical model under blue wavelengths (400 nm and 460 nm, Table 3), showing that metabolism could reduce ATP demand to match even the lowest ATP supply in BS. In this condition the ATP demand in BS was brought about by RuP phosphorylation and glyoxylate recycling, two processes that are known to be exclusive to BS. The predicted (ATP_{BS} + ATP_M) / GA was 5.74 (Fig. 4 B, dashed line), in agreement with J_{ATP} / GA measured under blue light (5.73, Fig. 4 B, blue square). Since photosynthetic PGA production is exclusive to BS (primarily from Rubisco carboxylase, or oxygenase activity and glyoxylate recycling), when there is no ATP available for PGA reduction, (e.g. in condition 1) the PGA diffuses to M and is reduced therein. After reduction, DHAP could supply starch synthesis in M or diffuse back to BS to regenerate RuBP. The predicted NADPH demand in BS ($NADPH_{BS}$) was therefore the lowest (Eqn. 14, Table 2; Fig. 4 A, dotted line), corresponding to

the NADPH demand for glyoxylate recycling in BS. The activity of malate dehydrogenase in M (MDH_M), process responsible for exporting NADPH, was reduced by diverting the substrate oxaloacetate (OAA) to transamination to aspartate (ASP). Hence, in condition 1, MDH_M had the lowest activity (Fig.1, Eqn. 16 in Table 2) while transamination had the highest rate (Fig. 1, Fig. 4 A, dashed line, Eqn 17 in Table 2). Once ASP diffused to BS, it underwent a futile reduction-oxidative decarboxylation that resulted in net CO_2 flux without a conjoint NADPH translocation (Fig. 1).

When PR and SS were progressively allocated in BS, the predicted ATP demand ATP_{BS} / ATP_M (Fig. 1, Fig. 4) progressively increased. The activation of PEPCK in BS, not only contributed to the predicted increasing ATP demand in BS, but also lowered the predicted ATP cost of assimilation (ATP_{BS} + ATP_M) / GA because PEPCK regenerates PEP with half the ATP demand of PPDK. Condition 2 (number 2 in Fig. 1 and Fig 4) represents a state where ATP_{BS} / ATP_M equals J_{ATPBS} / J_{ATPM} resolved from the optical model under red light (0.68, Table 3). The predicted (ATP_{BS} + ATP_M) / GA (5.45, Fig. 4 B, dashed line) agreed with J_{ATP} /GA measured under red light (5.47, Fig. 4 B, red square).

When the projected allocation of PR, PEPCK and SS to BS was highest (referred as condition 3, number 3 in Fig. 1, Fig. 4 A), the predicted ATP_{BS} / ATP_M was 0.8. This partitioning equals J_{ATPBS} / J_{ATPM} estimated by the optical model under green light, and it is similar to J_{ATPBS} / J_{ATPM} estimated under natural white light (0.76, Table 3). Because PEPCK was activated at a highest rate, only 70 % of PEP was regenerated through PPDK and (ATP_{BS} + ATP_M) / GA was lowest (5.39, Fig. 4 B, dashed line), predicting well J_{ATP} /GA values measured under RGB (5.38, Fig. 4 B, RGB square) and green light (5.37, Fig. 4 B, green square). In condition 3, PGA reduction in BS was highest, determining the highest $NADPH_{BS}$ (Fig. 1; Fig. 4 A dotted line; Eqn. 14, Table 2) and the highest MDH_M activity (Fig. 1, Eqn. 16 in Table 2). Because most of the OAA produced by PEP carboxylase was reduced by MDH_M, transamination rate was lowest, just enough to supply PEPCK activity in BS.

Estimate of actual reaction and diffusion rates.

Since all C_4 reactions were described by rate equations (Table 2) we could estimate actual reaction rates. Although the predictions shown so far (including the optical part) are largely independent of light intensity, in this step rates had to be calculated at a specific light intensity. However, in order to compare these values in a wider range of light intensities, rates were expressed as relative to GA. This was also functional to avoid any computational distortion caused by respiration in the vicinity of the light compensation point. The irradiance of 125 $\mu E\ m^{-2}\ s^{-1}$, characteristic of illumination in the shade, was chosen because ongoing studies on low light and light quality are relevant to the physiology of shading (see also discussion). Furthermore, since low light provides a mean to directly manipulate C_4 metabolism, a great deal of

comparable work has been undertaken both in this lab (Kromdijk et al., 2008; Kromdijk et al., 2010; Bellasio and Griffiths, 2013) and by other investigators (Ubierna et al., 2011; Ubierna et al., 2013) under low irradiances. Reaction rates, shown in the boxes within Fig. 1 were obtained by parameterizing the model with the data obtained during the experiment and with the output of the C_4 model [all equations are reported in Suppl. Table S 2 but see also (Bellasio and Griffiths, 2013), and references therein]. Rates were calculated for the three relevant conditions mentioned above, i.e. condition 1 corresponds to the lowest ATP demand in BS, condition 2 corresponds to an intermediate ATP demand (matching ATP supply under red light) while condition 3 correspond to the highest ATP demand in BS (matching ATP supply under green light). Condition 1, 2 and 3 were numbered 1, 2 and 3 in Fig. 1 and Fig. 4.

Discussion

The implications of the metabolic model for partitioning ATP demand are firstly considered in terms of previous studies of C_4 decarboxylases in NADP-ME systems. The resultant ATP partitioning and metabolic plasticity provided by these processes is then considered in terms of overall C_4 energetic limitations (Evans et al., 2007). Finally, we go on to consider the implications for multiple decarboxylase origins and function in terms of C_4 pathway evolution, as well as light use and energy partitioning within a C_4 crop canopy.

Modelling ATP demand: decarboxylase diversity in C_4 systems

Recent developments in C_4 research have highlighted the complexity of C_4 metabolism, in terms of extensive overlapping of BS and M functions (Friso et al., 2010; Majeran et al., 2010), the presence of two distinct decarboxylating pathways (Meister et al., 1996; Wingler et al., 1999; Pick et al., 2011), and plasticity in malate metabolism [(Eprintsev et al., 2011) and references therein]. Although an involvement in balancing the energetic capacity in responses to environmental conditions has been proposed (Eprintsev et al., 2011; Furbank, 2011), empirical evidence and an associated metabolic model were needed to validate this suggestion. In this study, we tested the capability of metabolism to respond to different ATP allocation between BS and M by means of a comprehensive metabolic model. To overcome uncertainties in the causal relationship between ATP availability and enzyme kinetics, we deduced the highest and lowest possible BS reaction rates from physiological considerations and studied how the predicted ATP demand partitioning ATP_{BS} / ATP_M would vary in response to incremental activation. We found that ATP_{BS} / ATP_M could vary between 0.27 to 0.80 if starch synthesis, PGA reduction (PR) and PEP regeneration were freely allocated between BS and M. In addition, we suggest that higher ATP consumption in BS than the predicted maximum, could result from the transient activation of PPDK in BS (Aoyagi and Nakamoto, 1985; Friso et al., 2010) or in a long-term response, from the de-novo synthesis of PR enzymes. This shows the importance of the presence of PPDK

in BS and the possibility of metabolism to regulate the maximum BS rate of PGA reduction in response to contrasting environmental conditions. These processes could take advantage of the increased ATP availability in BS under 540 nm green light (Table 3) or under high irradiances when ATP production in M is reduced (because of PSII yield quenching; Suppl. Fig. S 2).

The extensive overlap between BS and M functions was important for preserving the overall assimilation rate, and for any process activated in BS, a complementary decrease in M could rebalance overall metabolism so as the total rate of assimilation and ATP demand to remain constant in spite of contrasting BS / M engagement. In addition, we showed the importance of transamination (T) in balancing the reducing power needs in BS. When the ATP availability in BS was low (e.g. condition 1), PGA reduction in BS was down-regulated, and therefore there was a reduced NADPH demand in BS (Fig. 4 A, dotted line). Under these conditions, CO_2 was delivered to BS through ASP, a pathway that bypasses malate reduction in M and, hence, NADPH export to BS. This shift between ASP and MAL-mediated CCM indicates the importance of maintaining both pathways in NADP-ME subtype C_4 plants. The predicted T rate varied in response to environmental conditions from a minimum of 0.35 V_P to the entirety of the CO_2 delivered to BS, in line with the observation that ASP can support physiological rates of photosynthesis (Rathnam, 1978; Chapman and Hatch, 1981; Meister et al., 1996; Pick et al., 2011). Under white light, the model predicted a 33 % T / V_P, which is in line with radiolabelling and biochemical observations (Downton, 1970; Hatch, 1971; Chapman and Hatch, 1981). These predictions are not influenced by whether transamination is mediated by the 'conventional' glutamate aminotransferases (Fig. 1), or by the more recently documented aspartate aminotransferases (Pick et al., 2011), because, in the model, transamination is simply assumed to be a fast, passively regulated process at equilibrium.

Although a mechanistic explanation goes beyond the scope of this study, it is worth noting that the fine tuning between contrasting scenarios may be relatively straightforward at metabolic level. In fact, both the CCM and the RPP pathway share diffusible metabolites between BS and M cells and are mediated by fast reactions, which, in physiological conditions, are close to the thermodynamic equilibrium (e.g. transamination reactions or sugar phosphate conversions). The regulation of the fluxes may therefore be regulated in just a few key steps, for instance at the level of PGA reduction, or malate decarboxylation. These have long been known to be regulated by the stromal pH, by feedback from metabolite pools and by feed forward from light reactions (Johnson and Hatch, 1970; Drincovich and Andreo, 1994; Detarsio et al., 2003; Murmu et al., 2003; Trost et al., 2006; Eprintsev et al., 2011). The adjustment of the other reaction and diffusion rates may then follow passively, mediated by the feedback provided by changing relative metabolite concentrations in one or the other compartment.

Modelling ATP supply as a function of light quality

Previously, fluorescence microimaging had shown that, because of the characteristic C_4 concentric leaf anatomy, strongly absorbed blue wavelengths would result in preferential absorption in M cells as compared to wavelengths of light which could penetrate deeper into the leaf profile (Evans et al., 2007). However, difficulties in the interpretation of fluorescence imaging, which are dependent on the different fluorescence yield of PSI-rich-BS and PSII-rich-M, have prevented investigators from predicting the relative light harvesting in BS and M (Evans et al., 2007). To overcome these difficulties, we characterized the profiles of light penetration in a maize leaf by means of an absorption-scattering model, which represents a first attempt to calculate the extent of light absorption imbalance caused by light quality. Because both BS and M produce ATP in light reactions, light harvesting imbalances would alter ATP partitioning. These ATP production imbalances were estimated using the relative stoichiometry of the electron transport operating in BS and M. The effect was very different from the response to changing light intensity, in fact, light quality only marginally influenced the total ATP available at leaf level but resulted in a 3-fold difference in the fraction of ATP produced in the BS, from 0.29 to 0.96 (Table 3). These imbalances are potentially independent of the light intensity, however photochemical yield (i.e. quenching) was assumed independent of the position within the leaf (see also description of Eqn 3, below), an assumption which may not hold under high light intensity. Regulation of photosystem yield through the leaf profile (Terashima et al., 2009) might also occur under changing light quality. Differential quenching would represent an additional point of plasticity in response to changing light quality, which would have the effect of narrowing the window of possible ATP_{BS} / ATP_M. Since we were interested in biochemical plasticity in response to ATP imbalance rather than in detailing the mechanics of electron transport processes, we did not include the possible plasticity at thylakoid level, and hence maximised the operating range of possible ATP_{BS} / ATP_M variation.

This spatial partitioning of ATP production J_{ATPBS} / J_{ATPM} is different from the functional partitioning of ATP consumption of the C_4 model (von Caemmerer, 2000; Ubierna et al., 2011; Bellasio and Griffiths, 2013) and from the theoretical partitioning of ATP demand ATP_{BS} / ATP_M of the metabolic model presented here. In the C_4 model, the total ATP production, J_{ATP}, is simply assumed to be produced by an undivided electron transport chain (Yin and Struik, 2012), then partitioned to PEP regeneration activity or C_3 activity by a parameter known as x (Suppl. Table S 2). This operation does not involve spatial separations between BS and M. In this study we followed this conventional approach, which has been widely validated, then captured the partitioning between BS and M with the equations of the metabolic model (Table 2). On the basis of this division of work we calculated the theoretical partitioning of ATP demand ATP_{BS} / ATP_M. Values for ATP_{BS} / ATP_M were therefore derived independently from J_{ATPBS} / J_{ATPM} (J_{ATPBS} / J_{ATPM} was not used in model parameterization). These independently derived J_{ATPBS} / J_{ATPM} and ATP_{BS} / ATP_M were compared in Figure 4.

Implications for electron transport processes

To allow these ATP partitioning rearrangements there must be a high degree of flexibility at the electron transport chain level. In fact, although linear electron flow (LEF) activity in BS is often neglected [because of negligible expression of the O_2 evolving complex (Majeran and van Wijk, 2009; Friso et al., 2010) and non-appreciable O_2 evolving activity (Meierhoff and Westhoff, 1993)] evidence that appreciable linear flow can be supported by stromal reductants as glutathione and ascorbate has been presented (Walker and Izawa, 1979; Ivanov et al., 2001; Ivanov et al., 2005; Ivanov et al., 2007). These reductants are likely to be produced from NADPH, supplied by malate imported from M (Kanai and Edwards, 1999; Laisk and Edwards, 2000). These processes couple reductant pools at thylakoid and stromal level, and are likely to function as plasticity mechanisms, playing a pivotal role in acclimation to changing light conditions.

Most of the LEF activity is localized in M chloroplasts, which evolve O_2 and supply all reducing power requirements. For this reason, many reactions requiring NADPH (such as nitrogen reduction) are localised in M, to benefit from NADPH availability (Majeran et al., 2005). Even if M chloroplasts are specialized in NADPH production, the ratio of ATP versus NADPH demand is highly sensitive to BS / M assimilation partitioning (Figure 1). Meeting this variable requirement may involve differential engagement of LEF versus cyclic electron flow (CEF). The particular features of the CEF operating in maize (Ivanov et al., 2007; Laisk et al., 2010; Munekage et al., 2010; Hertle et al., 2013), may reflect, beyond the heterogeneity between BS and M specialization, this characteristic need for plasticity in CEF / LEF engagement.

Regardless of this electron transport plasticity, the ATP production deficits induced by changing light quality cannot be rebalanced within the individual BS chloroplast. In fact, increasing the ATP production at the electron transport chain level would require light (Takabayashi et al., 2005; Kramer and Evans, 2011), whose availability is not under metabolic control. At the same time, the electron transport mediated dark production of ATP (Morstadt et al., 2002; Bukhov and Carpentier, 2004; Egorova and Bukhov, 2004; Kuntz, 2004), has low conversion efficiency (Kramer and Evans, 2011), hence an engagement of ATP chemiosynthesis would be incompatible with the observed pattern of J_{ATP} / GA. ATP itself is not a suitable shuttle to rebalance ATP deficits because the ATP molecule is relatively big, it has a relatively small pool and homeostasis is critical, therefore every chloroplast has an independent ATP pool. Maintaining balanced ATP consumption in spite of local ATP deficits requires rearranging the localization of ATP demand, the fluxes, and the partitioning of metabolic work between the mutually interdependent BS and M cells.

Metabolic plasticity is effective in maintaining overall assimilation efficiency

Previously, on the basis of theoretical considerations, it had been predicted that an unbalanced ATP supply would result in a disruption of the delicate equilibrium between BS and M functions with consequent loss in assimilatory efficiency (Henderson et al., 1992; Evans et al., 2007; Tazoe et al., 2008). This prediction arose because metabolic rigidity would be expected under some of the common simplifications used for C_4 biochemistry, whereby transamination is neglected, PGA is reduced at a fixed rate in BS and NADPH delivery to BS is equimolar to CO_2 delivery (Laisk and Edwards, 2000; Laisk and Edwards, 2009). In the updated description of C_4 metabolism provided in this paper, reaction rates are variable and tuneable. When the ATP availability in BS was low (e.g. condition 1), PGA reduction in BS was downregulated, leaving all available ATP for RuBP regeneration, resulting in unaltered Rubisco efficiency. Because the ASP-mediated CCM delivers solely CO_2, while the MAL mediated CCM delivers both NADPH and CO_2, the variable engagement of the two pathways allows the activity of the CCM to be regulated independently of NADPH demand in BS, hence the optimal C_{BS} could be maintained under all light qualities.

These predictions are supported by further model outputs, where we found no significant effect of light quality on Φ and on C_{BS}, confirming the response found in a similar experiment where plants were acclimated under high light (Sun et al., 2011). This observation, together with the relatively minor change in J_{ATP} / GA (Fig. 4 B) show that C_4 metabolic balance was adjusting to the shifts in ATP supply without the potential major disruptions mentioned above.

Implications for light use at leaf and canopy level

Photosynthesis in shaded conditions has critical importance in C_4 canopies as it may represent up to 50 % of CO_2 uptake (Baker and Long, 1988; Long, 1993). Shade light has a reduced intensity [typically 1 / 20 of full sunlight (Shirley, 1929)], and differs in spectral quality from red-rich sunlight: diffuse sky radiation is enriched in blue, whereas canopy filtered light is enriched in green (Smith, 1982). Under low light conditions it has been shown that Φ may increase both at leaf e.g. (Kromdijk et al., 2010; Bellasio and Griffiths, 2013) and at canopy level (Kromdijk et al., 2008). Theoretical considerations have associated this Φ increase with decreased C_4 efficiency and a potential loss of photosynthetic carbon uptake (Furbank et al., 1990; von Caemmerer, 2000; Kromdijk et al., 2008; Tazoe et al., 2008). Although other studies have compared the effect of light quality on Φ under low irradiance or under different light qualities (Kromdijk et al., 2010; Sun et al., 2011; Bellasio and Griffiths, 2013; Ubierna et al., 2013), the novelty the approach presented here has been to couple the measured and predicted ATP supply during assimilation under these conditions. In this experiment, which was specifically optimized to acquire data under low light (Bellasio and Griffiths, 2013), we showed that the total ATP cost of gross assimilation was not significantly influenced by light intensity, and underwent a little variation under different light quality (Fig. 4 B). This showed that

metabolism at steady state under low light intensities, maintained efficiency in spite of changes in light quality or intensity. This implies that the hyperbolic increase of Φ observed under decreasing light intensities (Fig. 3 D), which underpins the predicted photosynthetic efficiency loss, actually did not cost additional ATP, but resulted instead from mitochondrial decarboxylation in BS (Bellasio and Griffiths, 2013). Similar conclusions were highlighted by (Ubierna et al., 2013). This observation is consistent with V_P / V_C and the optimal 'x' being largely independent of light intensity (von Caemmerer, 2000; Kromdijk et al., 2010), indicating a constant degree of engagement of the CCM even under an apparent leakiness increase. Care should therefore be taken when the ATP cost (and quantum yield) of C_4 photosynthesis is derived from Φ, measured either at leaf or canopy scale, particularly in the vicinity of the light compensation point (Furbank et al., 1990; von Caemmerer, 2000; Tazoe et al., 2008). In these conditions we propose that the ATP cost should be calculated by summing the ATP cost of all the active biochemical processes (e.g. Eqn 11, Table 2), instead of using leakiness as a proxy for C_4 biochemical efficiency. The actual impact of Φ on canopy-level carbon uptake may depend upon the extent of steady-state photosynthesis under low light or altered light quality conditions (e.g. green enriched), and shorter-term, more transient conditions, when Φ may be more variable.

Conclusion

In this study we set out to investigate whether the maize C_4 system could respond to changing environmental conditions by adjusting the C_4 (amino)acid (MAL or ASP) delivered from M to BS, as well as the proportions of other metabolic reactions shared between both cell types, such as starch synthesis, PGA reduction and PEP regeneration (Walker et al., 1986; Spilatro and Preiss, 1987; Wingler et al., 1999; Friso et al., 2010; Majeran et al., 2010; Furbank, 2011). Using contrasting light qualities and their projected extinction within the leaf profile, we could then estimate the rate of ATP synthesis in M and BS compartments, as compared to the overall leaf-level operating efficiency measured by gas exchange and real-time carbon isotope discrimination. We depicted a scenario whereby metabolism, although subject to the general constraints imposed by C_4 physiology, was able to take the maximum advantage of environmental conditions by changing the relative engagement of BS and M functions, which were ultimately under environmental control. The outputs, based on metabolic modelling and empirical measurements, provide definitive evidence for the role of complementarity between BS and M functions, allowing ATP demand to be regulated in response to contrasting environmental conditions. The two decarboxylase systems in BS of maize, with a variable rate of transamination, allow the regulation of NADPH supply to match demand in BS independently of the delivery of CO_2.

The findings of this study highlight the importance of C_4 metabolic models in helping to explain acclimation and adaptation to changing light intensity for all C_4 subgroups. The

463 emerging complexity of the NADP-ME / PEPCK interactions certainly demands some
464 refinement to the widespread simplifications used to describe C_4 systems and to the assumptions
465 regarding the relatively fixed energetic partitioning in maize. Furthermore, we have clearly
466 linked metabolic plasticity to the capacity to maintain high photosynthetic efficiency under
467 changing environmental conditions, which could well be related to original functions of bundle
468 sheath decarboxylases and evolution of the C_4 syndrome (Hibberd and Quick, 2002; Griffiths et
469 al., 2013). Finally, the extent that such steady state conditions of low light and altered light
470 quality affect carbon uptake within an intact crop canopy remain to be determined, as compared
471 to more transient responses which may well increase leakiness and reduce carbon assimilation
472 under low light conditions.

473 **Materials and Methods**

474 Metabolic model

475 The processes contributing to assimilatory metabolism in maize (Furbank, 2011) were
476 integrated in a comprehensive steady-state model (Fig. 1). Some functional simplifications were
477 made. Cells were decompartmentalized. NADPH and NADH were considered equivalent or
478 convertible. Starch was assumed to be the only final product of photosynthesis (starch synthesis
479 has the same ATP cost per hexose than phloem-loaded sucrose, considering the stoichiometry of
480 1 ATP / H^+ of the membrane H^+ - ATPase and 1 H^+ / sucrose of the sucrose synporter). The ATP
481 + NADH produced during respiration (assumed supplied by PGA) were neglected in calculations
482 because they are likely to be consumed by basal metabolism. Transamination (T) was assumed to
483 be passively regulated by substrate availability (all OAA not reduced by MDH was
484 transaminated), as T reactions are rapid conversions at equilibrium.
485 The specialization of BS and M was captured by assigning processes to BS, M, or to the
486 conjoint work of both compartments (allocatable processes). PEPCK (Walker et al., 1986;
487 Furumoto et al., 1999; Wingler et al., 1999; Furumoto et al., 2000) and glyoxylate recycling
488 (Yoshimura et al., 2004) were allocated to BS; linear electron flow (Meierhoff and Westhoff,
489 1993; Romanowska et al., 2006; Majeran and van Wijk, 2009; Friso et al., 2010; Kramer and
490 Evans, 2011) and PPDK (see discussion) were allocated to M; R_{LIGHT} was split equally between
491 M and BS (von Caemmerer, 2000; Kromdijk et al., 2010; Ubierna et al., 2011); PGA reduction
492 (PR) and starch synthesis (SS) were variably allocated. T rate was equal in BS and M as the pool
493 of ASP and ALA is shared. The model was described by steady state rate equations (Table 2).

494 Minimum and maximum BS allocation

495 The rate of variably allocated processes ranged between a minimum and maximum rate,
496 deduced from physiological considerations (but see discussion for the environmental influence

on maximum rates). Both BS and M express SS enzymes (Spilatro and Preiss, 1987; Majeran and van Wijk, 2009) and synthesize starch e.g. (Rascio et al., 1980; Kanai and Edwards, 1999), so SS was allocated to BS between 0 and SS_{TOT}. PR is not essential to BS so PR_{MIN} was set at 0. PR is mainly a M process (Majeran et al., 2005; Majeran and van Wijk, 2009), so PR_{MAX} was limited at $0.35 \cdot PR_{TOT}$. PEPCK is not essential to BS so $PEPCK_{MIN}$ was set at 0. $PEPCK_{MAX}$ was set at $0.3 \cdot V_P$, identified by fitting the total ATP demand of assimilation to J_{ATP} / GA (Fig. 4 B).

Parameterization

Equations describing overall assimilation (Eqn. 4 to 10, in Table 2), were parameterized with the measured data A, R_{LIGHT}, the output of the von Caemmerer C_4 model (V_O, V_P and V_C, Suppl. Table S 2) (Bellasio and Griffiths, 2013) and Φ calculated from Δ under PAR = 125 µE m^{-2} s^{-1} (see below). Then, reaction rates (Eqn. 4 to 21 in Table 2) were calculated under the minimum (condition 1) and the maximum (condition 3) BS allocation (Fig. 1 and Fig. 4 B). Finally, intermediate states (e.g. condition 2) were calculated by allocating reactions to BS in linear increments (see continuous lines in Fig. 4 A).

The ATP demand in BS (ATP_{BS}) was calculated by adding the ATP demand of BS processes (Table 2, Eqn. 12; Supp. Table S 1). Analogously, ATP_M was calculated by summing the ATP demand of M processes (Table 2, Eqn. 13; Supp. Table S 1), and the partitioning of ATP demand (ATP_{BS} / ATP_M) was calculated by dividing Eqn. 12 by Eqn. 13. Similarly the NADPH demand in BS ($NADPH_{BS}$) was calculated by summing the NADPH demand of BS processes (Table 2, Eqn. 14; Supp. Table S 1). Rate equations for other processes are listed in Table 2.

Estimated light harvesting in BS and M, AB BS / M

A maize leaf cross section was simulated by rectangular units, enclosing a square BS (left panel of Fig. 2). Inter-veinal distance (IVD, 106 µm); M thickness (100 µm), BS / M area (0.26) and the resulting BS side (46 µm) were averaged from (Hattersley, 1984; Usuda, 1985; BongardPierce et al., 1996; Moreno-Sotomayor et al., 2002; Kromdijk et al., 2010). Because of the square anatomy, the leaf light environment could be described by two light profiles: P1 and P2. These were calculated applying the Kubelka-Munk absorption – scattering theory with the method of Allen and Richardson (Allen and Richardson, 1968; Gates, 1980; Terashima et al., 2009), modified to describe the simulated C_4 anatomy. Briefly, each profile was considered to be made of a number n of light absorbing and scattering elements, the total number of elements in the profile was N. The element n=0 was the illuminated, or adaxial point of the profile, which included the upper epidermis, approximated to a single reflecting element. The element N was the abaxial point of the profile, which included the lower epidermis, approximated to a single reflecting element. Radiant flux directed downward was I, and that upward was J. Incident flux was I_0, and was taken to be the unity. For each profile, the flux reflected by the first element was

equivalent to the point reflectance and the flux transmitted by the last element was equivalent to the point transmittance: J(0) = Point refl. and I(N)= Point transm.

Incremental absorption and scattering were calculated as (Gates, 1980):

$$dI = -(k+s)Idn + sJdn \quad (1)$$

$$dJ = (k+s)Jdn - sIdn \quad (2)$$

Where k is an absorption coefficient and s is a scattering coefficient. In P1, k was constant throughout the profile. In P2 k was three times higher in the elements corresponding to BS, because chlorophyll concentration is three times higher than in the surrounding M [BS / M chl content, 0.74 (Kanai and Edwards, 1973), multiplied by M / BS area, 4; Fig. 2, left]. I and J were solved for all elements of P1 and P2 according to the integration of Eqn. 1 and 2 proposed by (Gates, 1980). Modelled leaf reflectance resulted from averaging J(0) contributions to the total leaf reflectance from P1 and P2 (56 % P1 and 44 % P2). Similarly, modelled leaf transmittance was calculated as a weighted average of I(N) from P1 and P2. Modelled leaf reflectance and transmittance were calibrated with measured leaf reflectance and transmittance at different wavelengths [Table 3, (Woolley, 1971)] by varying k and s. This procedure allowed calculating P1 and P2 at different wavelengths (Figure 2 right). Absorbed light (AB) in BS resulted from integrating P2 over BS area. AB in M resulted from integrating P2 over adaxial and abaxial mesophyll (MAD + MAB) area plus the integral of P1 over the two interveinal mesophyll (MI) areas.

Estimated ATP production partitioning, J_{ATPBS} / J_{ATPM}

M chloroplasts are engaged in NADPH and ATP production, therefore, for a given number of light quanta they produce c. half the ATP produced in BS chloroplast. J_{ATPBS} / J_{ATPM} was calculated as:

$$\frac{J_{ATPBS}}{J_{ATPM}} = 2 \cdot AB\frac{BS}{M} \quad (3)$$

The coefficient 2 (in Eqn. 3) is based on widely accepted assumption that light is equally shared between photosystems and on the simplification that the photochemical yield is independent of the position within the leaf profile. In detail we assumed: i) exclusive linear electron transport in M with equal PSI / PSII absorption partitioning (Meierhoff and Westhoff, 1993; Kramer and Evans, 2011); ii) exclusive cyclic electron transport in BS with no PSII absorption (Romanowska et al., 2006; Majeran and van Wijk, 2009); iii) equal yield of PSI and PSII (Miyake et al., 2005) (Supp. Fig. S 2 C); iv) equal H^+ / ATP stoichiometry of the ATP synthase in BS and M: the enzyme complex is the same (Majeran and van Wijk, 2009; Friso et al., 2010); v) twice the H^+ per photochemical event pumped in BS versus M: in M 1.5 H^+ are extruded per photochemical event (Kramer and Evans, 2011), while in BS we assumed 3 H^+ extruded per photochemical event [average between 4 H^+ of the NDH-mediated (Kramer and Evans, 2011; Peng et al., 2011) and 2 H^+ of the PGR5 / PGRL1-mediated electron flow (Kramer and Evans, 2011; Hertle et al., 2013) both operating in maize BS (Ivanov et al., 2007)].

Plants

Zea mays L. (F1 Hybrid PR31N27, Pioneer Hi-bred, Italy) plants were grown in 1.5 L pots filled with Levington pro M3 (Scotts, UK) in growth rooms (Conviron Ltd, Winnipeg, Canada) set at 16 h day length, temperature of 25 °C / 23 °C (day/night), 40 % relative humidity and PAR = 600 μE m^{-2} s^{-1} and manually watered daily with particular care to avoid overwatering. After three weeks plants were measured once and then discarded.

Gas exchange measurements with concurrent PSI / PSII Yield and on-line carbon isotopic discrimination *(Δ)*

The experimental setup was previously described (Bellasio and Griffiths, 2013). Briefly, an infra-red gas analyser (IRGA, a LI6400XT, Li-cor, USA), was fitted with a 6400-06 PAM2000 adapter, and with a Li-cor 6400-18 RGB light source. The IRGA was fed with CO_2 ($\delta^{13}C$ = -8.3 ‰, Isi, A) and either a mixture of 2 % O_2 / N_2 or ambient air. PS I yield and PS II yield, Y(II), were measured with a Dual Pam-F (Heinz Walz GmbH, Effeltrich, D). The IRGA was connected to a cryogenic H_2O and CO_2 trapping-purification line. To determine the relationship between Y(II) and J_{ATP}, a light response curve was measured at 2 % O_2 and C_a = 600 μmol / mol. Under the same light quality, 21 % O_2 and reference CO_2 set at 400 μmol / mol, a second light response curve was measured, during which Y(II) was determined and exhaust gas was trapped to determine *Δ*. In one day a total of 12 CO_2 samples and 6 CO_2 references from each individual plant were analysed directly with a VG SIRA dual inlet isotope ratio mass spectrometer (modified and maintained by Pro-Vac Services Ltd, Crewe, UK). *Δ* was calculated as reported in Supp. Fig. S 3, using Eqn. 22. R_{LIGHT} was calculated as the y-intercept of the linear regression of

A against PAR· Y(II) / 3. J_{ATP} was calculated from chlorophyll fluorescence data, by calibrating the relationship between ETR and Y(II) under low O_2, and then using such a calibration to determine the small fraction of ATP consumed by photorespiration. The correction was minimal because of the low O_2 sensitivity of maize [Suppl. Table S 2 (Bellasio and Griffiths, 2013)], therefore the potential errors caused by using fluorescence measurements under contrasting light qualities were negligible. Light responses were treated with dedicated software (Photosyn assistant 1.2, Dundee Scientific, Dundee, UK), to calculate the light compensation point and by repeated measures anova (Genstat), point estimates were subject to anova and Tukey multiple comparison (Genstat).

Leakiness Φ from isotopic discrimination Δ

Leakiness was resolved from isotopic discrimination by use of the full Farquhar model (Farquhar, 1983; Farquhar and Cernusak, 2012), parameterized with a C_4 photosynthesis model (von Caemmerer, 2000), using equations and a fitting approach that were previously described [Suppl. Table S 2 (Bellasio and Griffiths, 2013)]. Briefly, leakiness, Φ was resolved from Δ by calculating the weighted individual fractionations of the discriminating processes operating in C_4 photosynthesis. The CO_2 concentration in the cellular compartments was calculated by means of a C_4 model, parameterized with the light response data (A, Ci, Ca, J_{ATP}) and respiration in the light (R_{LIGHT}). The C_4 model was rearranged to express a modelled J_{MOD} and fit to the total ATP production rate J_{ATP} (Suppl. Table S 2), to yield a value for BS conductance for each individual plant, independently from Δ.

Acknowledgments

We are deeply grateful to Bernard Genty, Gerald Edwards and Joe Berry for discussion, to Julian Hibberd and Jessica Royles for review, to the Reviewers for the constructive feedback, and to Davide Gusberti for providing seeds.

References

Allen WA, Richardson AJ (1968) Interaction of Light with a Plant Canopy. Journal of the Optical Society of America **58:** 1023-&

Aoyagi K, Nakamoto H (1985) Pyruvate, Pi Dikinase in Bundle Sheath Strands as Well as in Mesophyll Cells in Maize Leaves. Plant Physiology **78:** 661-664

Baker NR, Long SP (1988) Photosynthesis and temperature, with particular reference to effects on quantum yield. *In* LS P, WF I, eds, Plants and temperature: Society for Experimental Biology Symposium No XXXXII. Company of biologists, pp 347-375

Barbour MM, McDowell NG, Tcherkez G, Bickford CP, Hanson DT (2007) A new measurement technique reveals rapid post-illumination changes in the carbon isotope composition of leaf-respired CO2. Plant Cell and Environment **30:** 469-482

Bellasio C, Griffiths H (2013) Acclimation to Low Light by C4 maize: Implications for Bundle Sheath Leakiness. Plant Cell and Environment **doi: 10.1111/pce.12194**

Berry JA, Farquhar GD (1978) The CO2 concentrating function of C4 photosynthesis: a biochemical model. *In* D Hall, J Coombs, T Goodwin, eds, Proceedings of the 4th International Congress on Photosynthesis. Biochemical Society, pp 119-131

BongardPierce DK, Evans MMS, Poethig RS (1996) Heteroblastic features of leaf anatomy in maize and their genetic regulation. International Journal of Plant Sciences **157:** 331-340

Bukhov N, Carpentier R (2004) Alternative Photosystem I-driven electron transport routes: mechanisms and functions. Photosynthesis Research **82:** 17-33

Chapman KSR, Hatch MD (1981) Aspartate Decarboxylation in Bundle Sheath-Cells of Zea-Mays and Its Possible Contribution to C-4 Photosynthesis. Australian Journal of Plant Physiology **8:** 237-248

Covshoff S, Hibberd JM (2012) Integrating C-4 photosynthesis into C-3 crops to increase yield potential. Current Opinion in Biotechnology **23:** 209-214

Craig H (1953) The Geochemistry of the Stable Carbon Isotopes. Geochimica Et Cosmochimica Acta **3:** 53-92

Detarsio E, Wheeler MCG, Bermudez VAC, Andreo CS, Drincovich MF (2003) Maize C(4)NADP-malic enzyme - Expression in Escherichia coli and characterization of site-directed mutants at the putative nucleotide-binding sites. Journal of Biological Chemistry **278:** 13757-13764

Downton WJS (1970) Preferential C4-dicarboxylic acid synthesis, the postillumination CO2 burst, carboxyl transfer step, and grana configurations in plants with C4-photosynthesis. Canadian Journal of Botany **48:** 1795-1800

Drincovich MF, Andreo CS (1994) Redox Regulation of Maize Nadp-Malic Enzyme by Thiol-Disulfide Interchange - Effect of Reduced Thioredoxin on Activity. Biochimica Et Biophysica Acta-Protein Structure and Molecular Enzymology **1206:** 10-16

Edwards GE, Baker NR (1993) Can CO2 assimilation in maize leaves be predicted accurately from chlorophyll fluorescence analysis. Photosynthesis Research **37:** 89-102

Egorova EA, Bukhov NG (2004) Modeling of alternative pathways of electron transport to photosystem I in isolated thylakoids. Russian Journal of Plant Physiology **51:** 579-583

Eprintsev AT, Fedorina OS, Bessmeltseva YS (2011) Response of the malate dehydrogenase system of maize mesophyll and bundle sheath to salt stress. Russian Journal of Plant Physiology **58:** 448-453

Evans JR, Sharkey TD, Berry JA, Farquhar GD (1986) Carbon Isotope Discrimination Measured Concurrently with Gas-Exchange to Investigate CO2 Diffusion in Leaves of Higher-Plants. Australian Journal of Plant Physiology **13:** 281-292

Evans JR, von Caemmerer S, Vogelmann TC (2007) Balancing light capture with distributed metabolic demand during C4 photosynthesis. *In* S J.E., M P.L., H B., eds, Charting new pathways to C4 rice. IRRI International Rice Research Institute

FAO (2012) Fao Statistical division web page, Rome. . *In*, www.fao.org

Farquhar GD (1983) On the Nature of Carbon Isotope Discrimination in C4 Species. Australian Journal of Plant Physiology **10:** 205-226

Farquhar GD, Cernusak LA (2012) Ternary effects on the gas exchange of isotopologues of carbon dioxide. Plant Cell and Environment **35:** 1221-1231

Friso G, Majeran W, Huang MS, Sun Q, van Wijk KJ (2010) Reconstruction of Metabolic Pathways, Protein Expression, and Homeostasis Machineries across Maize Bundle Sheath and Mesophyll Chloroplasts: Large-Scale Quantitative Proteomics Using the First Maize Genome Assembly. Plant Physiology **152:** 1219-1250

Furbank R, Jenkins C, Hatch M (1990) C4 Photosynthesis: Quantum Requirement, C4 and Overcycling and Q-Cycle Involvement. Functional Plant Biology **17:** 1-7

Furbank RT (2011) Evolution of the C4 photosynthetic mechanism: are there really three C4 acid decarboxylation types? Journal of Experimental Botany **62:** 3103-3108

Furumoto T, Hata S, Izui K (1999) cDNA cloning and characterization of maize phosphoenolpyruvate carboxykinase, a bundle sheath cell-specific enzyme. Plant Molecular Biology **41:** 301-311

Furumoto T, Hata S, Izui K (2000) Isolation and characterization of cDNAs for differentially accumulated transcripts between mesophyll cells and bundle sheath strands of maize leaves. Plant and Cell Physiology **41:** 1200-1209

Gates DM (1980) Biophysical Ecology. Springer Verlag, New York

Genty B, Briantais JM, Baker NR (1989) The relationship between the quantum yield of photosynthetic electron-transport and quenching of chlorophyll fluorescence. Biochimica Et Biophysica Acta **990:** 87-92

Ghashghaie J, Duranceau M, Badeck FW, Cornic G, Adeline MT, Deleens E (2001) δ13C of CO2 respired in the dark in relation to δ13C of leaf metabolites: comparison between Nicotiana sylvestris and Helianthus annuus under drought. Plant Cell and Environment **24:** 505-515

Gillon JS, Griffiths H (1997) The influence of (photo)respiration on carbon isotope discrimination in plants. Plant Cell and Environment **20:** 1217-1230

Griffiths H, Weller G, Toy LFM, Dennis RJ (2013) You're so vein: bundle sheath physiology, phylogeny and evolution in C3 and C4 plants. Plant, Cell & Environment **36:** 249-261

Hatch MD (1971) The C 4 -pathway of photosynthesis. Evidence for an intermediate pool of carbon dioxide and the identity of the donor C 4 -dicarboxylic acid. Biochem. J. **125:** 425-432

Hattersley PW (1984) Characterization of C-4 Type Leaf Anatomy in Grasses (Poaceae), Mesophyll - Bundle Sheath Area Ratios. Annals of Botany **53:** 163-179

Henderson SA, Von Caemmerer S, Farquhar GD (1992) Short-Term Measurements of Carbon Isotope Discrimination in Several C4 Species. Australian Journal of Plant Physiology **19:** 263-285

Hertle AP, Blunder T, Wunder T, Pesaresi P, Pribil M, Armbruster U, Leister D (2013) PGRL1 Is the Elusive Ferredoxin-Plastoquinone Reductase in Photosynthetic Cyclic Electron Flow. Molecular Cell **49:** 511-523

Hibberd JM, Quick WP (2002) Characteristics of C4 photosynthesis in stems and petioles of C3 flowering plants. Nature **415:** 451-454

Hymus GJ, Maseyk K, Valentini R, Yakir D (2005) Large daily variation in C-13-enrichment of leaf-respired CO2 in two Quercus forest canopies. New Phytologist **167:** 377-384

Igamberdiev AU, Mikkelsen TN, Ambus P, Bauwe H, Lea PJ, Gardestrom P (2004) Photorespiration contributes to stomatal regulation and carbon isotope fractionation: a study with barley, potato and Arabidopsis plants deficient in glycine decarboxylase. Photosynthesis Research **81:** 139-152

Ivanov B, Asada K, Edwards GE (2007) Analysis of donors of electrons to photosystem I and cyclic electron flow by redox kinetics of P700 in chloroplasts of isolated bundle sheath strands of maize. Photosynthesis Research **92:** 65-74

Ivanov B, Asada K, Kramer DM, Edwards G (2005) Characterization of photosynthetic electron transport in bundle sheath cells of maize. I. Ascorbate effectively stimulates cyclic electron flow around PSI. Planta **220:** 572-581

Ivanov BN, Sacksteder CA, Kramer DM, Edwards GE (2001) Light-induced ascorbate-dependent electron transport and membrane energization in chloroplasts of bundle sheath cells of the C-4 plant maize. Archives of Biochemistry and Biophysics **385:** 145-153

Johnson HS, Hatch MD (1970) Properties and Regulation of Leaf Nicotinamide-Adenine Dinucleotide Phosphate-Malate Dehydrogenase and Malic Enzyme in Plants with C4-Dicarboxylic Acid Pathway of Photosynthesis. Biochemical Journal **119:** 273-&

Kanai R, Edwards GE (1973) Separation of Mesophyll Protoplasts and Bundle Sheath Cells from Maize Leaves for Photosynthetic Studies. Plant Physiology **51:** 1133-1137

Kanai R, Edwards GE (1999) The biochemistry of C4 photosynthesis. *In* RF Sage, RK Monson, eds, C4 plant biology. Academic Press, San Diego

Kramer DM, Evans JR (2011) The Importance of Energy Balance in Improving Photosynthetic Productivity. Plant Physiology **155:** 70-78

Kromdijk J, Griffiths H, Schepers HE (2010) Can the progressive increase of C4 bundle sheath leakiness at low PFD be explained by incomplete suppression of photorespiration? Plant Cell and Environment **33:** 1935-1948

Kromdijk J, Schepers HE, Albanito F, Fitton N, Carroll F, Jones MB, Finnan J, Lanigan GJ, Griffiths H (2008) Bundle Sheath Leakiness and Light Limitation during C4 Leaf and Canopy CO2 Uptake. Plant Physiology **148:** 2144-2155

Kuntz M (2004) Plastid terminal oxidase and its biological significance. Planta **218:** 896-899

Laisk A, Edwards G (2009) Leaf C4 Photosynthesis in silico: The CO2 Concentrating Mechanism. *In* A Laisk, L Nedbal, Govindjee, eds, Photosynthesis in silico, Vol 29. Springer Netherlands, pp 323-348

Laisk A, Edwards GE (2000) A mathematical model of C-4 photosynthesis: The mechanism of concentrating CO2 in NADP-malic enzyme type species. Photosynthesis Research **66:** 199-224

Laisk A, Talts E, Oja V, Eichelmann H, Peterson RB (2010) Fast cyclic electron transport around photosystem I in leaves under far-red light: a proton-uncoupled pathway? Photosynthesis Research **103:** 79-95

Lanigan GJ, Betson N, Griffiths H, Seibt U (2008) Carbon Isotope Fractionation during Photorespiration and Carboxylation in Senecio. Plant Physiology **148:** 2013-2020

Long SP (1993) The significance of light-limited photosynthesis to crop canopy carbon gain and productivity - a theoretical analysis. *In* YP Abrol, P Mohanty, Govindjee, eds, Photosynthesis: Photoreactions to Plant Productivity. Oxford & IBH publishing, New Delhi, pp 547 - 560

Majeran W, Cai Y, Sun Q, van Wijk KJ (2005) Functional Differentiation of Bundle Sheath and Mesophyll Maize Chloroplasts Determined by Comparative Proteomics. The Plant Cell Online **17:** 3111-3140

Majeran W, Friso G, Ponnala L, Connolly B, Huang MS, Reidel E, Zhang CK, Asakura Y, Bhuiyan NH, Sun Q, Turgeon R, van Wijk KJ (2010) Structural and Metabolic Transitions of C-4 Leaf Development and Differentiation Defined by Microscopy and Quantitative Proteomics in Maize. Plant Cell **22:** 3509-3542

Majeran W, van Wijk KJ (2009) Cell-type-specific differentiation of chloroplasts in C4 plants. Trends in Plant Science **14:** 100-109

Meierhoff K, Westhoff P (1993) Differential Biogenesis of Photosystem-Ii in Mesophyll and Bundle-Sheath Cells of Monocotyledonous Nadp-Malic Enzyme-Type C-4 Plants - the Nonstoichiometric Abundance of the Subunits of Photosystem-Ii in the Bundle-Sheath Chloroplasts and the Translational Activity of the Plastome-Encoded Genes. Planta **191:** 23-33

Meister M, Agostino A, Hatch MD (1996) The roles of malate and aspartate in C-4 photosynthetic metabolism of Flaveria bidentis (L). Planta **199:** 262-269

Miyake C, Miyata M, Shinzaki Y, Tomizawa K-i (2005) CO2 Response of Cyclic Electron Flow around PSI (CEF-PSI) in Tobacco Leaves—Relative Electron fluxes through PSI and PSII Determine the Magnitude of Non-photochemical Quenching (NPQ) of Chl Fluorescence. Plant and Cell Physiology **46:** 629-637

Mook WG, Bommerso.Jc, Staverma.Wh (1974) Carbon Isotope Fractionation between Dissolved Bicarbonate and Gaseous Carbon-Dioxide. Earth and Planetary Science Letters **22:** 169-176

Moreno-Sotomayor A, Weiss A, Paparozzi ET, Arkebauer TJ (2002) Stability of leaf anatomy and light response curves of field grown maize as a function of age and nitrogen status. Journal of Plant Physiology **159:** 819-826

Morstadt L, Graber P, de Pascalis L, Kleinig H, Speth V, Beyer P (2002) Chemiosmotic ATP synthesis in photosynthetically inactive chromoplasts from Narcissus pseudonarcissus L. linked to a redox pathway potentially also involved in carotene desaturation. Planta **215:** 134-140

Munekage YN, Eymery F, Rumeau D, Cuine S, Oguri M, Nakamura N, Yokota A, Genty B, Peltier G (2010) Elevated Expression of PGR5 and NDH-H in Bundle Sheath Chloroplasts in C-4 Flaveria Species. Plant and Cell Physiology **51:** 664-668

Murmu J, Chinthapalli B, Raghavendra AS (2003) Light activation of NADP malic enzyme in leaves of maize: Marginal increase in activity, but marked change in regulatory properties of enzyme. Journal of Plant Physiology **160:** 51-56

O'Leary MH (1984) Measurement of the isotope fractionation associated with diffusion of carbon dioxide in aqueous solution. The Journal of Physical Chemistry **88:** 823-825

Peng L, Yamamoto H, Shikanai T (2011) Structure and biogenesis of the chloroplast NAD(P)H dehydrogenase complex. Biochimica et Biophysica Acta (BBA) - Bioenergetics **1807:** 945-953

Pick TR, Brautigam A, Schluter U, Denton AK, Colmsee C, Scholz U, Fahnenstich H, Pieruschka R, Rascher U, Sonnewald U, Weber APM (2011) Systems Analysis of a Maize Leaf Developmental Gradient Redefines the Current C-4 Model and Provides Candidates for Regulation. Plant Cell **23:** 4208-4220

Rascio N, Colombo PM, Orsenigo M (1980) The ultrastructural development of plastids in leaves of maize plants exposed to continuous illumination. Protoplasma **102:** 131-139

Rathnam CKM (1978) Studies with Isolated Bundle Sheath Mitochondria - Evidence for Nad-Malic Enzyme-Catalyzed Decarboxylation of C4 Acids in Species Representing 3 C4 Metabolic Subtypes. Febs Letters **96:** 367-372

Roeske CA, Oleary MH (1984) Carbon Isotope Effects on the Enzyme-Catalyzed Carboxylation of Ribulose Bisphosphate. Biochemistry **23:** 6275-6284

Romanowska E, Drozak A, Pokorska B, Shiell BJ, Michalski WP (2006) Organization and activity of photosystems in the mesophyll and bundle sheath chloroplasts of maize. Journal of Plant Physiology **163:** 607-618

Sage RF, Sage TL, Kocacinar F (2012) Photorespiration and the evolution of C4 photosynthesis. Annual review of plant biology **63:** 19-47

Schulze S, Mallmann J, Burscheidt J, Koczor M, Streubel M, Bauwe H, Gowik U, Westhoff P (2013) Evolution of C-4 Photosynthesis in the Genus Flaveria: Establishment of a Photorespiratory CO2 Pump. Plant Cell **25:** 2522-2535

Shirley HL (1929) The Influence of Light Intensity and Light Quality Upon the Growth of Plants. American Journal of Botany **16:** 354-390

Smith H (1982) Light Quality, Photoperception, and Plant Strategy. Annual Review of Plant Physiology **33:** 481-518

Spilatro SR, Preiss J (1987) Regulation of starch synthesis in the bundle sheath and mesophyll of Zea mays L. Intercellular compartmentalization of enzymes of starch metabolism and the properties of the ADPglucose pyrophosphorylases. Plant Physiology **83:** 621-627

Sun W, Ubierna N, Ma J-Y, Cousins AB (2011) The influence of light quality on C4 photosynthesis under steady-state conditions in Zea mays and Miscanthus× giganteus: changes in rates of photosynthesis but not the efficiency of the CO2 concentrating mechanism. Plant, Cell & Environment**:** no-no

Sun WEI, Ubierna N, Ma J-Y, Cousins AB (2012) The influence of light quality on C4 photosynthesis under steady-state conditions in Zea mays and Miscanthus × giganteus: changes in rates of photosynthesis but not the efficiency of the CO2 concentrating mechanism. Plant, Cell & Environment **35:** 982-993

Takabayashi A, Kishine M, Asada K, Endo T, Sato F (2005) Differential use of two cyclic electron flows around photosystem I for driving CO2-concentration mechanism in C-4 photosynthesis. Proceedings of the National Academy of Sciences of the United States of America **102:** 16898-16903

Tazoe Y, Hanba YT, Furumoto T, Noguchi K, Terashima I (2008) Relationships between quantum yield for CO2 assimilation, activity of key enzymes and CO2 leakiness in Amaranthus cruentus, a C4 dicot, grown in high or low light. Plant and Cell Physiology **49:** 19-29

Tazoe YS, Noguchi K, Terashima I (2006) C-4 photosynthetic efficiency under low light in Amaranthus cruentus L.: The relationship between CO2 leakiness and in vivo activities of C-4 photosynthetic enzymes. Plant and Cell Physiology **47:** S210-S210

Terashima I, Fujita T, Inoue T, Chow WS, Oguchi R (2009) Green Light Drives Leaf Photosynthesis More Efficiently than Red Light in Strong White Light: Revisiting the Enigmatic Question of Why Leaves are Green. Plant and Cell Physiology **50:** 684-697

Trost P, Fermani S, Marri L, Zaffagnini M, Falini G, Scagliarini S, Pupillo P, Sparla F (2006) Thioredoxin-dependent regulation of photosynthetic glyceraldehyde-3-phosphate dehydrogenase: autonomous vs. CP12-dependent mechanisms. Photosynthesis Research **89:** 263-275

Ubierna N, Sun W, Cousins AB (2011) The efficiency of C4 photosynthesis under low light conditions: assumptions and calculations with CO2 isotope discrimination. Journal of Experimental Botany **62:** 3119-3134

Ubierna N, Sun W, Kramer DM, Cousins AB (2013) The Efficiency Of C4 Photosynthesis Under Low Light Conditions In Zea Mays, Miscanthus X Giganteus And Flaveria Bidentis. Plant, Cell & Environment **36:** 365-381

Usuda H (1985) Changes in Levels of Intermediates of the C-4 Cycle and Reductive Pentose-Phosphate Pathway during Induction of Photosynthesis in Maize Leaves. Plant Physiology **78:** 859-864

Vogel JC (1980) Fractionation of the carbon isotopes during photosynthesis. Springer, Berlin and New york

Vogel JC, Grootes PM, Mook WG (1970) Isotopic Fractionation between Gaseous and Dissolved Carbon Dioxide. Zeitschrift Fur Physik **230:** 225-238

von Caemmerer S (2000) Biochemical models of leaf Photosynthesis. Csiro

von Caemmerer S (2013) Steady-state models of photosynthesis. Plant, Cell & Environment **36:** 1617-1630

von Caemmerer S, Farquhar GD (1981) Some Relationships between the Biochemistry of Photosynthesis and the Gas-Exchange of Leaves. Planta **153:** 376-387

Walker GH, Izawa S (1979) Photosynthetic Electron-Transport in Isolated Maize Bundle Sheath-Cells. Plant Physiology **63:** 133-138

Walker GH, Ku MSB, Edwards GE (1986) Activity of Maize Leaf Phosphoenolpyruvate Carboxylase in Relation to Tautomerization and Nonenzymatic Decarboxylation of Oxaloacetate. Archives of Biochemistry and Biophysics **248:** 489-501

Wingate L, Seibt U, Moncrieff JB, Jarvis PG, Lloyd J (2007) Variations in 13C discrimination during CO2 exchange by Picea sitchensis branches in the field. Plant Cell and Environment **30:** 600-616

Wingler A, Walker RP, Chen ZH, Leegood RC (1999) Phosphoenolpyruvate carboxykinase is involved in the decarboxylation of aspartate in the bundle sheath of maize. Plant Physiology **120:** 539-545

Woolley JT (1971) Reflectance and Transmittance of Light by Leaves. Plant Physiology **47:** 656-662

Yin XY, Struik PC (2012) Mathematical review of the energy transduction stoichiometries of C4 leaf photosynthesis under limiting light. Plant Cell and Environment **35:** 1299-1312

Yoshimura Y, Kubota F, Ueno O (2004) Structural and biochemical bases of photorespiration in C-4 plants: quantification of organelles and glycine decarboxylase. Planta **220:** 307-317

Zhu X-G, Long SP, Ort DR (2010) Improving photosynthetic efficiency for greater yield. Annual review of plant biology **61:** 235-261

Tables.

Table 1. Abbreviations, definitions and units for variables and acronyms described in the text.

A	Net assimilation	μmol m^{-2} s^{-1}
AB	Absorbed light	
AB BS / M	Partitioning of absorbed light	dimentionless
ALA	Alanine	
ASP	Aspartate	
ATP	Adenosine 5' triphosphate	
ATP_{BS}	ATP demand in BS	μmol m^{-2} s^{-1}
ATP_{M}	ATP demand in M	μmol m^{-2} s^{-1}
B	Blue	
BS	Bundle sheath	
C_{BS}	CO_2 concentration in BS	μmol mol^{-1}
CCM	Carbon concentrating mechanism	
CEF	Cyclic electron flow	
DHAP	Dihydroxyacetone phosphate	
ETR	Electron transport rate	μmol m^{-2} s^{-1}
G	Green	
GA	Gross assimilation (A + R_{LIGHT})	μmol m^{-2} s^{-1}
g_{BS}	Bundle sheath conductance to CO2, calculated by fitting J_{MOD} to J_{ATP}	mol m^{2} s^{-1}
GLA	Glycolic acid	
IRGA	Infra-red gas analyzer	
IVD	Inter veinal distance	μm
J_{ATP}	Total ATP production rate	μmol m^{-2} s^{-1}
J_{ATPBS}	ATP production rate in BS	μmol m^{-2} s^{-1}
J_{ATPM}	ATP production rate in M	μmol m^{-2} s^{-1}
J_{MOD}	Modelled ATP production rate	μmol m^{-2} s^{-1}
LEF	Linear electron flow	
LCP	Light compensation point	
M	Mesophyll	
MAL	Malic acid	
MDH	Malate dehydrogenase	
MDH_{BS}	Malate dehydrogenase reaction rate in BS	μmol m^{-2} s^{-1}
MDH_{M}	Malate dehydrogenase reaction rate in M	μmol m^{-2} s^{-1}
ME	Malic enzyme	
ME	Malic enzyme reaction rate	μmol m^{-2} s^{-1}
NADPH	Nicotinamide adenine dinucleotide phosphate	
$NADPH_{BS}$	NADPH demand in BS	μmol m^{-2} s^{-1}
$NADPH_{TOT}$	Total NADPH demand	μmol m^{-2} s^{-1}
OAA	Oxaloacetic acid	
PAR	Photosynthetically active radiation	μE m^{-2} s^{-1}
PEP	Phosphoenolpyruvate	
PEPCK	Phosphoenolpyruvate carboxykinase	
$PEPCK$	PEPCK reaction rate	μmol m^{-2} s^{-1}
PGA	3-phosphoglyceric acid	
PGLA	2-phosphoglycolic acid	
PPDK	Pyruvate phosphate dikinase	
$PPDK$	PPDK reaction rate	μmol m^{-2} s^{-1}
PR	PGA reduction	
PR_{BS}	PGA reduction rate in BS	μmol m^{-2} s^{-1}
PR_{M}	PGA reduction rate in M	μmol m^{-2} s^{-1}
PSI	Photosystem I	
PSII	Photosystem II	
PYR	Pyruvic acid	
R	Red	
R_{BS}	Respiration in the light in BS	μmol m^{-2} s^{-1}
R_{LIGHT}	Respiration in the light	μmol m^{-2} s^{-1}
R_{M}	Respiration in the light in M	μmol m^{-2} s^{-1}
RPP	Reductive pentose phosphate	
Rubisco	Ribulose bisphosphate carboxylase oxygenase	
RuBP	Ribulose-1,5-bisphosphate	
RuP	Ribulose-5-phosphate	
SS	Starch synthesis	
SS_{BS}	Starch synthesis rate in BS	μmol m^{-2} s^{-1}
SS_{M}	Starch synthesis rate in M	μmol m^{-2} s^{-1}
SS_{TOT}	Total starch synthesis rate	μmol m^{-2} s^{-1}
T	Transamination	
T	Transamination rate	μmol m^{-2} s^{-1}
V_C	Rubisco carboxylation rate	μmol m^{-2} s^{-1}
V_O	Rubisco oxygenation rate	μmol m^{-2} s^{-1}
V_P	PEP carboxylation rate	μmol m^{-2} s^{-1}
$Y(II)$	Yield of photosystem II	
Δ	^{13}C Isotopic discrimination	‰
$\delta^{13}C$	^{13}C isotopic composition relative to Pee dee belemnite	‰
Φ	Leakiness	dimentionless

Table 2. Steady state equations for the metabolic model of C_4 assimilation. Processes described by Eqn. 4 to 10 can be calculated directly from the measured data A, R_{LIGHT} and the output of the von Caemmerer C_4 model (V_O, V_P and V_C), while Eqn. from 11 to 21 require prior allocation of starch synthesis (SS), PGA reduction (PR) and PEPCK. For simplicity, enzyme names in italics represent the enzyme reaction rate. For stoichiometric consistency, reaction rates are calculated as rates of substrate transformation.

Process	Symbol	Reaction rate	Eqn.	Localization	Notes
Gross assimilation	GA	$A + R_{LIGHT}$	**(4)**		*GA* and R_{LIGHT} rates are expressed per CO_2
RuP phosphorylation	-	$V_c + V_O$	**(5)**	BS	RuP phosphorilation supplies Rubisco carboxylating activity (V_C), together with oxygenating activity (V_O).
PGA reduction tot	PR_{TOT}	$2V_C + \frac{3}{2}V_O - \frac{R_{LIGHT}}{3}$	**(6)**	BS and M	This equation calculates the total rate of PGA reduction on the basis of the PGA produced by Rubisco carboxylation ($2V_C$), Rubisco oxygenation (V_O) and glyoxylate recycling ($0.5V_O$) and considers the PGA consumed by respiration. 1/3 is the stoichiometric conversion between respiration (expressed per CO_2) and PR (expressed per triose).
NADPH demand tot	$NADPH_{TOT}$	$PR_{TOT} + \frac{1}{2}V_O$	**(7)**	BS and M	PGA reduction consumes 1 NADPH per PGA. The total rate of PGA reduction is PR_{TOT} (see note to Eqn 6). In glyoxylate regeneration (per glyoxylate) 0.5 NADH is produced by glycine decarboxylase, 0.5 NADH is consumed by hydroxypyruvate reductase and one ferredoxin (equivalent to 0.5 NADPH) is consumed by glutamine synthetase. In total 0.5 NADPH is consumed per glyoxylate formed (equivalent to V_O rate, see Table S 2) (Yoshimura et al., 2004).
DHAP entering RPP	-	$PR_{TOT} - SS_{TOT}$	**(8)**	BS	The DHAP entering the RPP pathway corresponds to the total PGA reduction rate minus the DHAP used for starch synthesis, which in this work is expressed per triose.
Starch synthesis tot	SS_{TOT}	$\frac{A}{3}$	**(9)**	BS and M	In this model all net assimilation is converted to starch. This assumption does not influence energetics as starch synthesis has the same ATP demand as phloem-loaded sucrose. In Eqn 9, 1/3 converts the stoichiometry of *A* (expressed per CO_2) to the stoichiometry of *SS* (expressed per triose).
PEP regeneration tot	-	V_P	**(10)**	BS and M	PEP regeneration rate equals PEP consumption rate V_P at steady state. PEP can be regenerated either by PPDK (mainly in M, but active also in BS) or by PEPCK in BS. In this study PPDK activity was assumed to be zero in BS
ATP demand tot	ATP_{BS} + ATP_M	$PR_{TOT} + V_C + 2V_O + \frac{1}{2}SS_{TOT} + PEPCK + 2PPDK$	**(11)**	BS and M	Eqn 11 calculates the total ATP demand as the sum of ATP demand for PGA reduction (1 ATP per PGA corresponding to *PR*), RuBP regeneration (1 ATP per RuP corresponding to V_C+V_O), glyoxylate recycling (1 ATP per glyoxylate, corresponding to V_O), starch synthesis (0.5 ATP per triose, corresponding to *SS*) and PEP regeneration (1 ATP per PEPCK catalytic event or 2 ATP per PPDK catalytic event). Compared to the original formulation of the C4 model, Eqn 11 separates the ATP demand for PEPCK and PPDK, it includes the ATP demand for SS, and considers the PGA utilised by respiration which does not need to be reduced (see Eqn 6).
ATP demand in BS	ATP_{BS}	$PR_{BS} + V_c + 2\,V_O + \frac{1}{2}\,SS_{BS} + PEPCK$	**(12)**	BS	The ATP demand in BS is brought about by PGA reduction (at the rate of PR_{BS}), RuBP regeneration (at the rate of V_C + V_O), glyoxylate recycling (at the rate of V_O), starch synthesis (0.5 ATP per triose) and PEPCK activity (1 ATP per OAA) (see note to Eqn 11).
ATP demand in M	ATP_M	$2\,PPDK + \frac{1}{2}\,SS_M + PR_M$	**(13)**	M	The ATP demand in M is brought about by PGA reduction (at the rate of PR_M), starch synthesis and PPDK (2 ATP per PYR) (see note to Eqn 11).
NADPH demand in BS	$NADPH_{BS}$	$PR_{BS} + \frac{1}{2}V_O$	**(14)**	BS	The NADPH demand in BS is brought about by PGA reduction (1 NADPH per PGA) and glyoxylate recycling, which consumes 0.5 NADPH per glyoxylate (corresponding to V_O, see also Suppl. Table S 1).
NADPH supply to BS	-	MDH_M	**(15)**	BS	All NADPH available in BS is produced in M and exported through the malate shuttle because we have assumed that no LET (i.e. water oxidation) occurred in BS. For this reason, the NADPH supply to BS corresponds to the NADPH consumed to reduce OAA to MAL in M, the process responsible for NADPH export, and not to the rate of MAL decarboxylation in BS, which depends on *T*, *PEPCK* and MDH_{BS} (Eqn. 19).
MDH activity in M	MDH_M	$PR_{BS} + \frac{1}{2}V_O$	**(16)**	M	MDH activity supplies the NADPH demand in BS. Eqn 16 was derived from Eqn 14 and 15.
Transamination	T	$V_P - MDH_M$	**(17)**	BS and M	Eqn 17 expresses that at steady state all OAA is either transaminated or reduced. Since *T* bypasses the MDH_M reaction, which is the reaction responsible for NADPH export to BS (see note to Eqn 15), *T* has the function of balancing NADPH supply and demand, this becomes apparent when Eqn 15 and 17 are combined.
Malate dehydrogenase	MDH_{BS}	*T-PEPCK*	**(18)**	BS	MDH is assumed to operate a fast conversion at equilibrium therefore it is passively regulated by the substrate availability: the OAA that is not used by PEPCK is reduced to MAL by MDH. MDH may use NADH, since no NADPH dependent reduction of OAA has been observed in maize (Kanai and Edwards, 1999) and it is likely mitochondrial (Rathnam, 1978; Chapman and Hatch, 1981). The NADH regeneration may be carried out by chloroplastic ME which is reported to react both with NADP and NAD (Chapman and Hatch, 1981), However the process may be more complicated [(Eprintsev et al., 2011) and references therein]. Note that in this study we assumed that cells are decompartmentalized while PEPCK rate was manipulated to increase between 0 and a maximum rate in response to ATP availability (see minimum and maximum BS allocation for details).
Malic enzyme	*ME*	MDH_M+MDH_{BS}	**(19)**	BS	Eqn 19 expresses that the rate of MAL oxidation by ME corresponds to the rate of MAL produced by MDH activity in M plus the rate of MAL produced by MDH activity in BS.
Pyruvate phosphate dikinase	*PPDK*	V_P-*PEPCK*	**(20)**	M	The PEP regenerated by PEPCK in BS diffuses to M and reduces the requirement of PEP regenerated by PPDK in M.
PGA reduction M	PR_M	PR_{TOT} - PR_{BS}	**(21)**	M	PGA reduction is a shared process between BS and M.

Table 3. Energy partitioning between BS and M at different wavelengths. Measured leaf reflectance and transmittance (Woolley, 1971) was used to parameterize the optical model (Fig. 2) to calculate the likely profiles of light penetration at different wavelengths. Absorbed light partitioning (AB BS / M) was calculated integrating such light absorption profiles (Fig. 2, right panel) over the corresponding BS and M areas (Fig. 2 left) and used to calculate ATP production partitioning J_{ATPBS} / J_{ATPM}.

Wavelength	Description	Refl. %	Transm. %	$AB\frac{BS}{M}$	$\frac{J_{ATPBS}}{J_{ATPM}}$
400 nm	Lowest $AB\frac{BS}{M}$	4	0.1	0.15	0.29
460 nm	Blue LED used	5	1	0.16	0.31
635 nm	Red LED used	6	7	0.34	0.68
400 – 700 nm	Natural white light	8	9	0.38	0.76
522 nm	Green LED used	8	11	0.40	0.80
540 nm	Highest $AB\frac{BS}{M}$	13	23	0.48	0.96

Table 4. Physiological responses of maize plants to different light qualities. The light compensation point (LCP) was determined by fitting light curves with dedicated software; Respiration in the light (R_{LIGHT}) was determined by linear regression of A against PAR·Y(II) / 3; bundle sheath conductance (g_{BS}) was determined by fitting a modelled J_{ATP} to the measured J_{ATP} (Fig. 3). Differences were not significant for $P < 0.05$. Mean values ± SE. n = 4

	Unit	Mean	RGB	R	G	B
LCP	µE m^{-2} s^{-1}	29.04	28.05 (± 1.8)	21.24 (± 3.1)	33.10 (± 4.1)	33.75 (± 5.7)
R_{LIGHT}	µmol O_2 m^{-2} s^{-1}	1.169	1.202 (± 0.090)	1.231 (± 0.11)	1.148 (± 0.11)	1.095 (± 0.12)
g_{BS}	mol m^{-2} s^{-1}	0.00104	0.00127 (± 3.1•10^{-4})	0.00117 (± 3.1•10^{-4})	0.00075 (± 3.1•10^{-4})	0.00247 (± 3.1•10^{-4})

Figures

Fig. 1. Metabolic model of C_4 assimilation, rates of reaction, and net fluxes between BS and M. The overall scheme reports the reactions of the CCM (Furbank, 2011), Rubisco carboxylation, the reactions of the RPP pathway, the synthesis of starch, respiration and glyoxylate recycling reactions. The tables, with the corresponding enzyme name, show the actual reaction rates, expressed as relative to GA (5.13 μmol /m^{-2} s^{-1}), per unit of substrate transformed. Rates were estimated by parameterizing the model equations (Table 2) with data measured under PAR = 125 μE m^{-2} s^{-1} (A = 3.96 μmol m^{-2} s^{-1}; R_{LIGHT} = 1.17 μmol m^{-2} s^{-1}; J_{ATP} = 28.6 μmol m^{-2} s^{-1}), the output of the C_4 model (V_C=5.35 μmol m^{-2} s^{-1}; V_P=5.89 μmol m^{-2} s^{-1}; V_O=0.44 μmol m^{-2} s^{-1}) and the output of the isotopic discrimination model (Φ = 0.23), under three characteristic ratios of ATP partitionings. These were numbered 1, 2 and 3. Condition 1 corresponds to the lowest ATP available in BS (ATP partitioning similar to that under blue light, Fig. 4 B), condition 2 correspond to an intermediate ATP availability in BS (ATP partitioning equal to that under red light, Fig. 4 B), condition 3 corresponds to the highest ATP available in BS (ATP partitioning equal to that under green light, Fig. 4 B). The inset shows net metabolite fluxes between M and BS in multiples of GA. The ATP demand in BS (ATP_{BS}) and M (ATP_M), the total NADPH demand ($NADPH_{TOT}$) and the NADPH demand in BS ($NADPH_{BS}$) were also calculated in the same three relevant conditions.

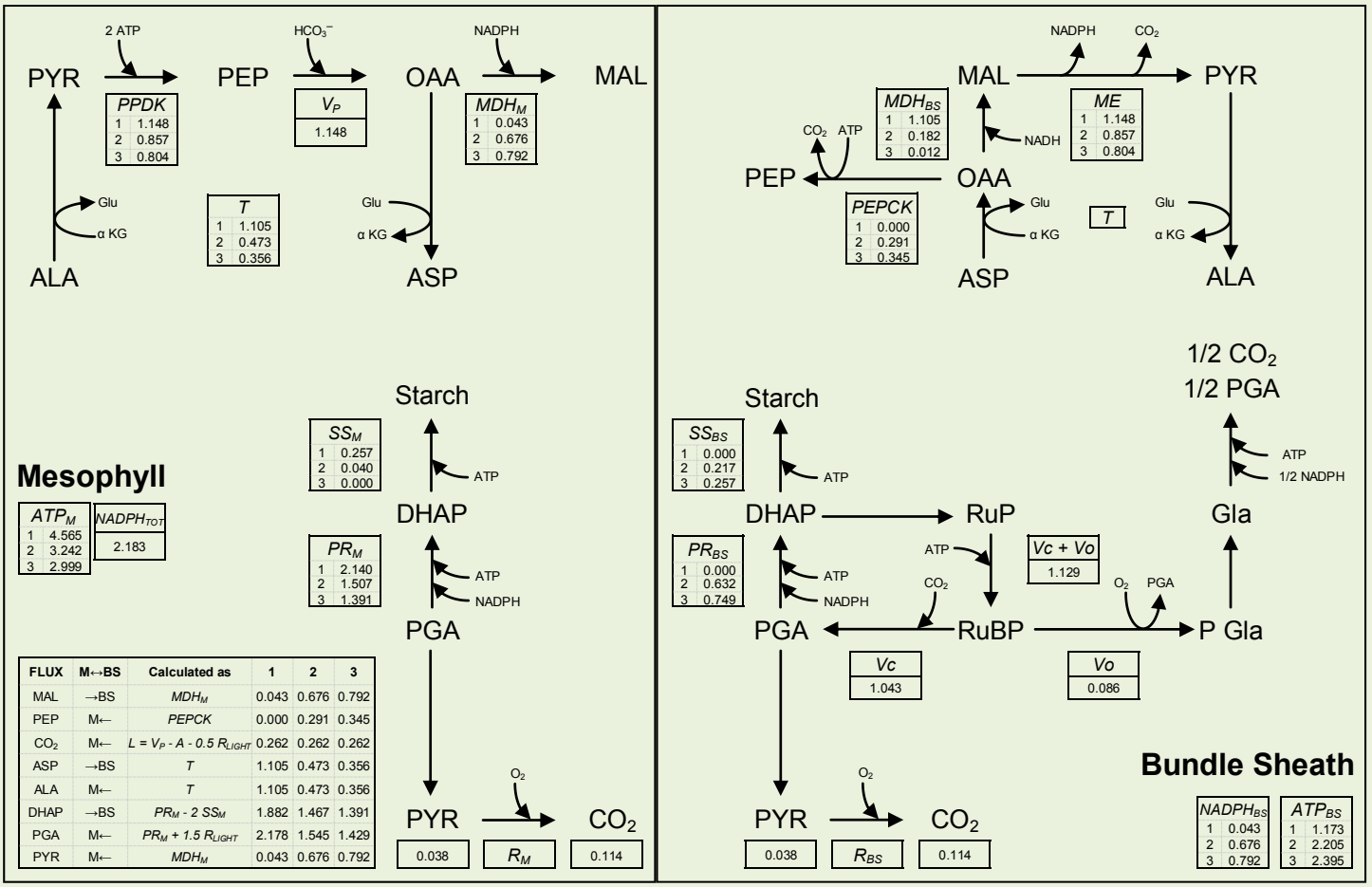

Fig. 2. Light penetration in a maize leaf. Left panel shows the modelled maize anatomy. A square BS is surrounded by three portions of mesophyll: interveinal mesophyll (MI), adaxial mesophyll (MAD) and abaxial mesophyll (MAB). Epidermis was approximated as a flat reflecting surface. Light penetration was studied through profiles P1 and P2. Right panel shows P1-light profiles (bold lines) and P2-light profiles (thin lines) calculated with the Kubelka-Munk (absorption + scattering) theory and calibrated with spectroscopic data (Table 3). Radiation is expressed as the sum of downward + upward photon flux, as a fraction of incident photon flux (dimentionless), and plotted against the depth in the absorbing path of the leaf.

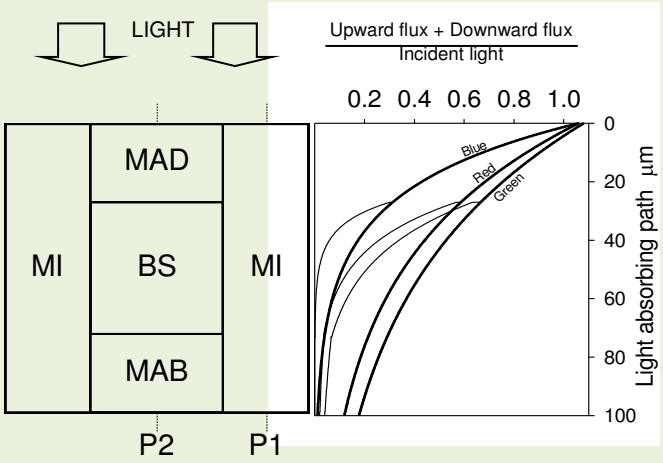

Fig. 3. Maize responses to decreasing light intensity under different light qualities. **(A)** Net assimilation (A). The curves were fitted in order to calculate the light compensation point (Table 4). The inset shows a magnification. **(B)** Total ATP production rate (J_{ATP}), measured with the low O_2 - ETR method. **(C)** On-line isotopic discrimination during photosynthesis (Δ). **(D)** Leakiness (Φ) resolved from Δ. Error bars represent standard error. n=4.

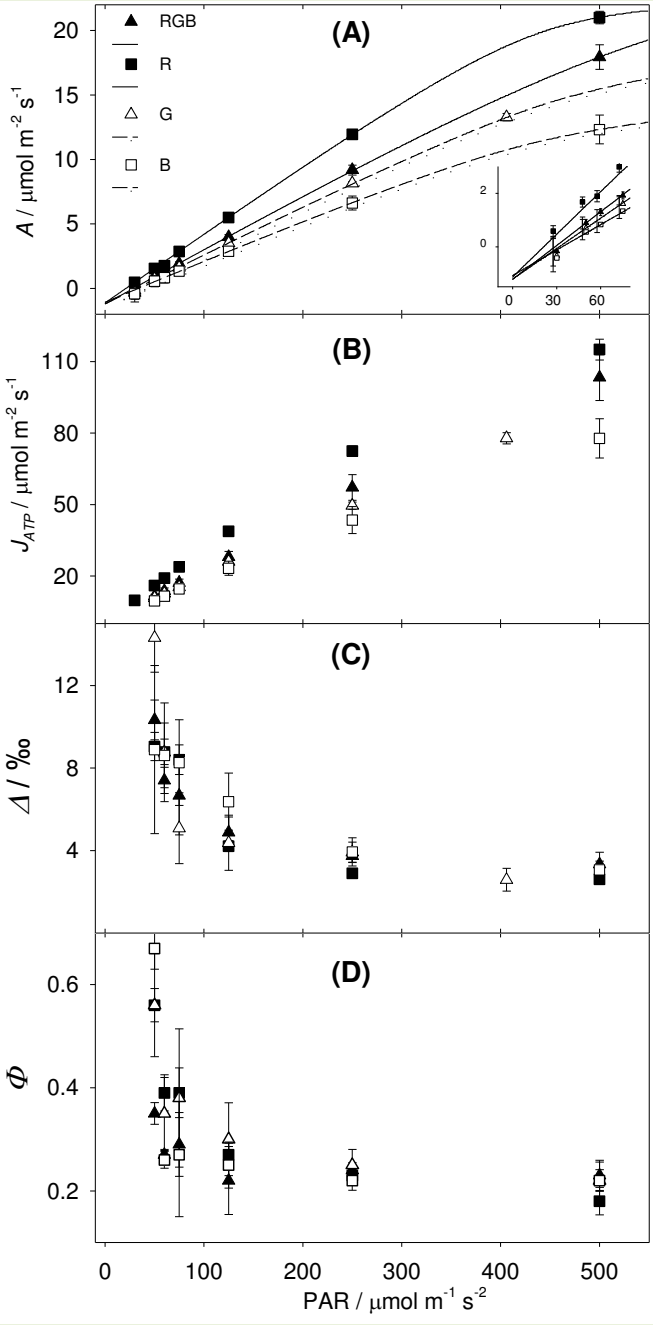

Fig. 4. Partitioning of metabolic activities in BS cells and associated shifts in ATP and NADPH demand. Panel (A), the output of the metabolic model, shows as a function of increasing theoretical ATP demand partitioning (ATP_{BS} / ATP_M), i) the increasing contribution of BS (solid lines) to the total PGA reduction (PR, relative to the total), starch synthesis (SS, relative to the total) and PEPCK (relative to the highest rate); ii) the predicted NADPH demand in BS, relative to the total ($NADPH_{BS}$ / $NADPH_{TOT}$, dotted line), and iii) the predicted transamination rate, relative to V_P (T / V_P, dashed line). In panel (B) the output of the metabolic model is compared with the empirical data. Model output is shown by a dashed line: the predicted ATP demand for gross assimilation (ATP_{BS} + ATP_M) / GA is plotted as a function of predicted ATP demand partitioning ATP_{BS} / ATP_M. Empirical data are shown as diamonds: the measured J_{ATP} / GA, under blue, red, RGB and green light (Table 1), is plotted against the estimated ATP production partitioning J_{ATPBS} / J_{ATPM} at 460 nm, 635 nm, white light and 522 nm (estimated through the optical model, Table 3). The lowest ATP_{BS} / ATP_M was named condition 1 (left arrow), the partitioning corresponding to red light was named condition 2 (central arrow) while the highest ATP_{BS} / ATP_M was named condition 3 (right arrow).

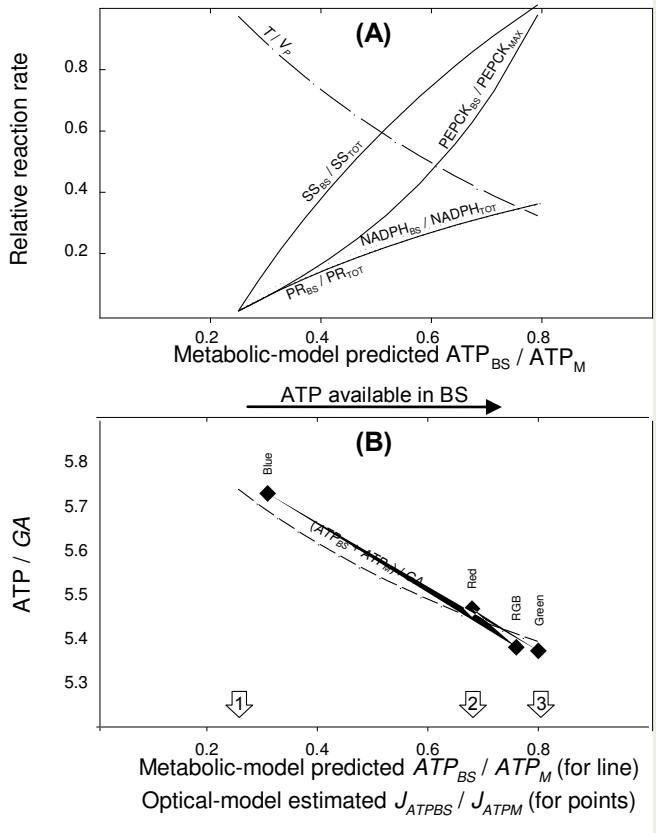

Supplementary Table S 1. ATP and NADPH demand for key C_4 processes.

Process	Localization	Per	ATP	NADPH
PGA reduction to DHAP	M+BS	PGA	1	1
RuP phosphorylation	BS	pentose	1	
Glyoxylate regeneration	BS	Glyoxylate	1	0.5
Starch synthesis	M+BS	triose	0.5	
PEPCK		OAA	1	
PPDK	M	PYR	2	

Supplementary Table S 2. Definitions, equations, and variables used in the models.

Symbol	Definition	Values / Units / References
a	^{13}C fractionation due to diffusion of CO_2 in air. Because of vigorous ventilation we neglected the fractionation of the boundary layer (Kromdijk *et al.*, 2010).	4.4 ‰ (Craig, 1953)
a_d	^{13}C fractionation due to diffusion of CO_2 in water	0.7 ‰ (O'Leary, 1984)
b_3	^{13}C fractionation during carboxylation by Rubisco including respiration and photorespiration fractionation $b_3 = b'_3 - \frac{e\prime \cdot R_{LIGHT} + f \cdot F}{V_c}$ (Farquhar, 1983). Where F is the photorespiration rate and was calculated as F=0.5·V_O [(von Caemmerer, 2013), Nerea Ubierna, personal communication]	‰
b_3'	^{13}C fractionation during carboxylation by Rubisco	30 ‰ (Roeske and Oleary, 1984)
b_4	Net fractionation by CO_2 dissolution, hydration and PEPC carboxylation including respiratory fractionation $b_4 = b'_4 - \frac{e\prime R_M}{V_P}$ (Farquhar, 1983; Henderson et al., 1992).	‰
b_4'	Net fractionation by CO_2 dissolution, hydration and PEPC carboxylation.	-5.7 ‰ at 25 °C but variable with temperature (Farquhar, 1983; Henderson et al., 1992; Kromdijk et al., 2010).
C_{BS}	CO_2 concentration in the bundle sheath $C_{BS} = \frac{\frac{xJ_{ATP}}{2} - \frac{R_{LIGHT}}{2} - A}{g_{BS}} + C_M$	µmol mol^{-1}
C_M	CO_2 concentration in the mesophyll $C_M = C_i - \frac{A}{g_M}$	µmol mol^{-1}
C_i	CO_2 concentration in the intercellular spaces as calculated by the IRGA (Li-cor manual Eqn 1-18).	µmol mol^{-1}
e	^{13}C fractionation during decarboxylation	0 ‰ to -10 ‰ (Gillon and Griffiths, 1997; Ghashghaie et al., 2001; Igamberdiev et al., 2004; Hymus et al., 2005; Barbour et al., 2007; Sun et al., 2012), -6 ‰ in this study (Kromdijk *et al.*, 2010).
e'	^{13}C fractionation during decarboxylation, including the correction for measurement artefacts: $e' = e + \delta\,^{13}C_{measurements} - \delta\,^{13}C_{growth\,chamber}$ In this study $\delta^{13}C_{measurements}$ = -6.38 ‰; $\delta^{13}C_{growth\ chamber}$ = -8 ‰ (Wingate *et al.*, 2007)	‰
e_s	^{13}C fractionation during internal CO_2 dissolution	1.1 ‰ (Vogel et al., 1970; Mook et al., 1974; Vogel, 1980).
f	^{13}C fractionation during photorespiration.	-11.6 ‰ (Lanigan *et al.*, 2008).
g_{BS}	Bundle sheath conductance to CO_2, calculated by curve fitting	mol m^2 s^{-1}
g_M	Mesophyll conductance to CO_2	1 mol m^2 s^{-1} bar^{-1} (Kromdijk *et al.*, 2010)
g_s	Stomata conductance to CO_2	mol m^2 s^{-1}
J_{ATP}	ATP production rate $J_{ATP} = \frac{3\,GA_{Low\,O_2}\,Y(II)}{0.59\,Y(II)_{Low\,O_2}}$	µmol m^{-2} s^{-1} (Bellasio and Griffiths, 2013)
J_{MOD}	Modelled ATP production rate $J_{MOD} = \frac{-y + \sqrt{y^2 - 4wz}}{2w}$ $w = \frac{x - x^2}{6A}$; $y = \frac{1-x}{3}\left[\frac{g_{BS}}{A} + \left(C_M - \frac{R_M}{g_{BS}} - \gamma^* O_M\right) - 1 - \frac{\alpha\gamma^*}{0.047}\right] - \frac{x}{2}\left(1 + \frac{R_{LIGHT}}{A}\right)$; $z = \left(1 + \frac{R_{LIGHT}}{A}\right)\left(R_M - g_{BS}\,C_M - \frac{7\,g_{BS}\,\gamma^* O_M}{3}\right) + (R_{LIGHT} + A)\left(1 - \frac{7\alpha\gamma^*}{3 \cdot 0.047}\right)$	µE m^{-2} s^{-1}µm (von Caemmerer, 2000; Bellasio and Griffiths, 2013; Ubierna et al., 2013)
O_M	O_2 mol fraction in the mesophyll cells (in air at equilibrium)	210000 µmol mol^{-1}
O_{BS}	O_2 mol fraction in the bundle sheath cells (in air at equilibrium) $O_{BS} = O_M + \frac{\alpha A}{0.047\,g_{BS}}$ (von Caemmerer, 2000)	µmol mol^{-1}
R_M	Mesophyll non photorespiratory CO_2 production in the light R_M = 0.5 R_{LIGHT} (von Caemmerer, 2000; Kromdijk et al., 2010; Ubierna et al., 2011)	µmol m^{-2} s^{-1}
s	Fractionation during leakage of CO_2 out of the bundle sheath cells	1.8 ‰ (Henderson *et al.*, 1992).
t	Ternary effects $t = \frac{(1+a)\,E}{2000\,g_{ac}}$ where E / mmol m^{-2} s^{-1} is the transpiration rate (calculated by the IRGA software, parameter Trmmol), g_{ac} / mol m^{-2} s^{-1} is the conductance to diffusion of CO_2 in air (calculated by the IRGA software, parameter CndCO2), a is the isotopic fractionation during diffusion in air.	‰ (Farquhar and Cernusak, 2012)
V_C	Rubisco carboxylation rate $V_C = \frac{(A + R_{LIGHT})}{1 - \frac{\gamma^* O_{BS}}{C_{BS}}}$ (Ubierna *et al.*, 2011)	µmol m^{-2} s^{-1}
V_O	Rubisco oxygenation rate $V_O = \frac{V_C - A - R_{LIGHT}}{0.5}$ (Ubierna *et al.*, 2011)	µmol m^{-2} s^{-1}
V_P	PEP Carboxylation rate $V_P = \frac{x]_{ATP}}{2}$	
Φ	Leakiness estimated with the isotope method including respiratory and photorespiratory fractionation, ternary effects and estimating CBS with the C_4 model $\Phi = \frac{C_{BS} - C_M}{C_M} \frac{b_4 C_M (1+t) + a(C_a - C_i) - C_a \Delta_{OBS}(1-t)}{(1+t)[C_a \Delta_{OBS}(1-t) - a(C_a - C_i) - b_3 C_{BS} + s(C_{BS} - C_M)]}$	dimentionless (Farquhar and Cernusak, 2012)
x	Partitioning factor of J_{ATP} between C4 activity V_P and C3 activity (reductive pentose phosphate pathway, RuBP regeneration and photerespiratory cycle)	0.4 (von Caemmerer, 2000; Kromdijk et al., 2010; Ubierna et al., 2011; Ubierna et al., 2013)
α	Fraction of PSII active in BS cells	0.15 (Edwards and Baker, 1993; von Caemmerer, 2000; Kromdijk et al., 2010).
γ^*	Half of the reciprocal of the Rubisco specificity	0.000193 (von Caemmerer, 2000).
$Y(II)$	Yield of photosystem II $Y(II) = \frac{F'_m - F_s}{F'_m}$ (Genty *et al.*, 1989)	dimentionless

Supplementary Fig. S 1. (A) Stomatal conductance and **(B)** Ci / Ca responses measured by gas exchange under decreasing light intensity, and under different light qualities. **(C)**: response of C_{BS} to decreasing light intensity, under different light qualities, estimated by the C_4 model. Error bars represent standard error. n=4.

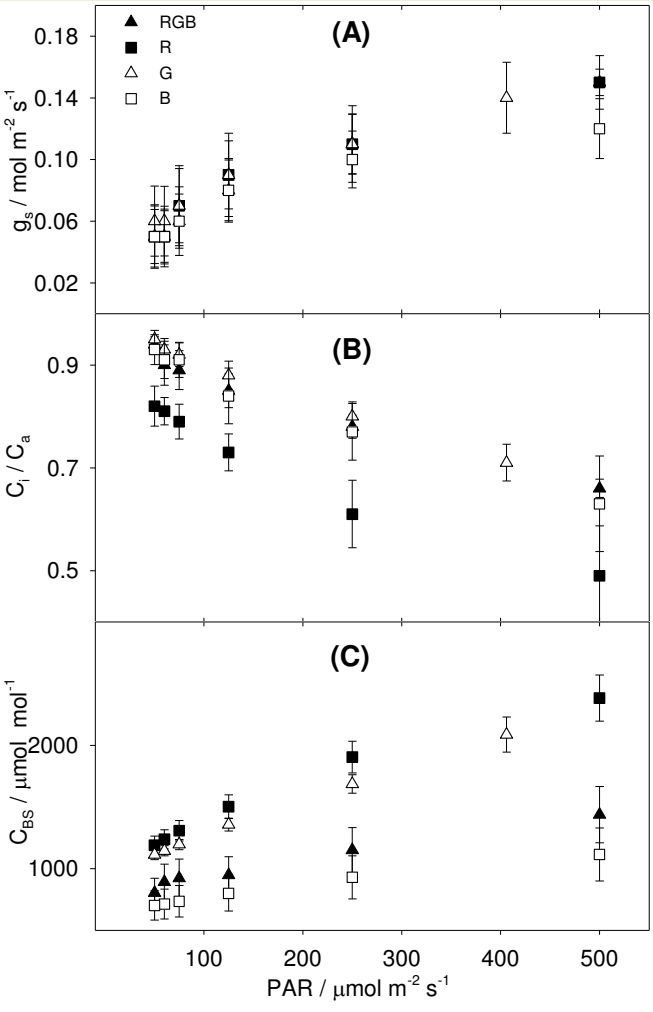

Supplementary Fig. S 2. Maize photochemical responses to decreasing light intensity under different light qualities. **(A)** Yield of photosystem I, determined with the low O_2-Electron Transport Rate method (Bellasio and Griffiths, 2013) **(B)** Yield of photosystem II, Y(II), determined by chlorophyll fluorescence. **(C)** Y(I) / Y(II). Error bars represent standard error. n=4.

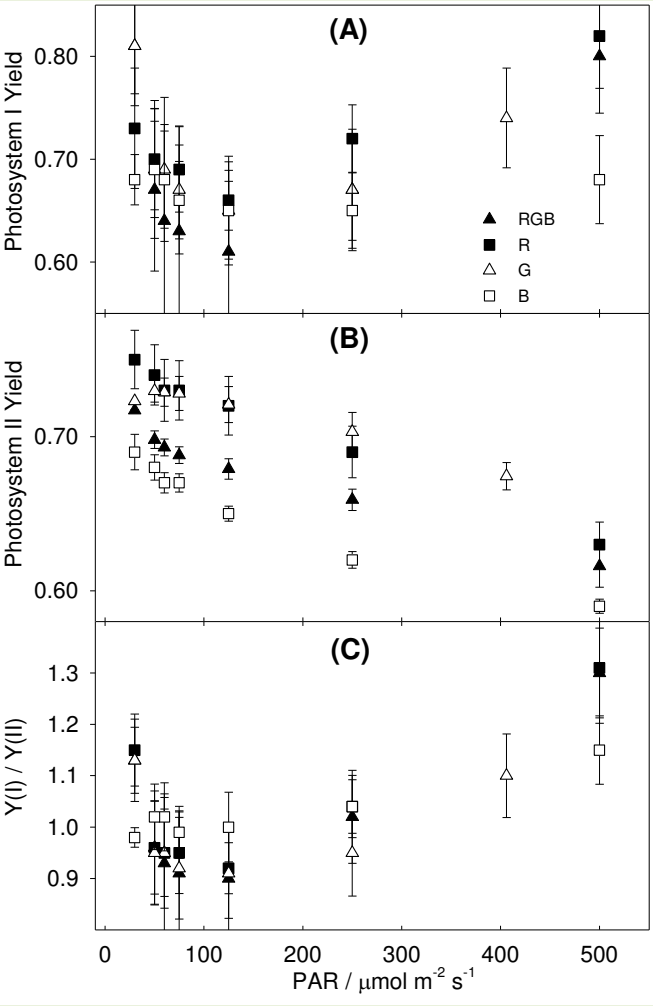

Supplementary Fig. S 3. values for the calculation of Δ.

Δ was calculated as (Evans et al., 1986):

$$\Delta_{OBS} = \frac{\xi(\delta_o - \delta_e)}{1 + \delta_o - \xi(\delta_o - \delta_e)} \quad \textbf{(22)}$$

Where: $\xi = \frac{C_e}{C_e - C_o}$; δ_e is the isotopic composition of the reference gas. δ_o is the isotopic composition of the gas leaving the cuvette. C_e and C_o represent the CO_2 mole fraction respectively entering and leaving the cuvette. These were corrected for differences in water content according to (von Caemmerer and Farquhar, 1981).